NAIST-IS-DD0461046

Doctoral Dissertation

Estimating Diffuse and Specular Reflectance Parameters from Spectral Images

Shiying Li

February 1, 2007

Department of Information Processing
Graduate School of Information Science
Nara Institute of Science and Technology

A Doctoral Dissertation
submitted to Graduate School of Information Science,
Nara Institute of Science and Technology
in partial fulfillment of the requirements for the degree of
Doctor of ENGINEERING

Shiying Li

Thesis Committee:

Professor	(Supervisor) Kunihiro Chihara
Professor	(Co-supervisor) Naokazu Yokoya
Associate Professor	(Supervisor) Yoshitsugu Manabe

Estimating Diffuse and Specular Reflectance Parameters from Spectral Images *

Shiying Li

Abstract

Reflection properties of an object, such as color and gloss, are essential surface characteristics for distinguishing one object from another. Important subjects in computer graphics and vision are how to acquire intrinsic information about colors and gloss of a real object without the influence of the measurement environment, and how to estimate accurate reflectance parameters, so as to reproduce reflection properties of the object in applications such as preserving cultural heritage in a digital museum, exhibiting commercial goods for online shops, and creating augmented environments with imaginary and real objects for entertainment.

Estimation of reflectance parameters is dependent on the quality of input images captured by a commercial imaging detector. However, most imaging detectors are based on red, green, and blue (RGB) trichromatic theory. RGB images may be inadequate representations of the intrinsic spectral distribution of reflected light at the surface of an object, because of effects such as metamerism. Another problem is that imaging detectors have a limited dynamic range, as a result of which an obtained image is often too dark in some areas and perhaps saturated in others. In either of such cases, information about colors and texture may be measured inaccurately, especially in glossy areas where the intensity of specular reflection is beyond the limited dynamic range of the detectors.

To solve these two problems, and to estimate diffuse and specular reflectance parameters accurately, two approaches are developed in the present work. First,

*Doctoral Dissertation, Department of Information Processing, Graduate School of Information Science, Nara Institute of Science and Technology, NAIST-IS-DD0461046, February 1, 2007.

a new measurement system has been constructed to capture spectral images of an object as input images, instead of RGB color images, using an imaging spectrograph, which is equipped with a monochrome charge coupled device (CCD) camera, and a light source, which is rotated around the object between -90^o and 90^o. After removing the influence of spectral power distribution of the light source and properties of the CCD camera, reflection values are separated into diffuse and specular reflection components at each wavelength for each surface point using spectral images, and diffuse reflectance parameters are estimated at each wavelength along with the separation.

Second, two methods have been developed to estimate specular reflectance parameters for gloss intensity and for surface roughness of an object from saturated specular reflection components, one by assuming Fresnel reflectance as a constant value, the other by estimating Fresnel reflectance. The equation of the Torrance-Sparrow reflection model is transformed logarithmically to a linear form, and the least squares method is then applied to the specular reflection components that are lower than a threshold.

Experiments were conducted using synthetic reflection values, with or without noise, and using measured spectral images of objects with different reflection properties at their surfaces. The experimental results have demonstrated that by applying these methods, diffuse reflectance parameters for color can be estimated accurately at each wavelength, and specular reflectance parameters for gloss intensity and for surface roughness can be estimated efficiently from either unsaturated or saturated specular reflection components, requiring neither color segmentation nor synthesis of high dynamic range images.

Keywords:

Reflectance parameters, Specular reflection, Diffuse reflection, Spectral images, Color, Gloss

Contents

List of Figures

List of Tables

Chapter 1

Introduction

1.1. Background

Throughout the world, there are enormous numbers of cultural heritage artifacts from previous generations, which are irreplaceable assets for all humankind. Some of the materials of these artifacts are fragile, such as glass and ceramics; some are perishable and combustible, such as wood and paper; and all are susceptible to wars, earthquakes, floods, or simply the passage of time. Therefore, it is a significant challenge for present and future generations to record the surface characteristics, as well as shapes, of cultural heritage artifacts in digital form, so that they can be preserved semipermanently and made available via the Internet and multimedia technology for both normal and academic applications.

In addition to virtual museums and art galleries, online shopping (also known as electronic commerce, internet shopping, and virtual shopping) has become commonplace in people's everyday lives since the late 1990s. Customers can browse products, e.g., ceramic goods and clothes, on the website of an online store, pick out their favorite items and check them out as they do in a physical store, according to the appearance of the products and descriptive information. On the other hand, in games and films, many scenes are augmented with imaginary and real objects for highly realistic sensation and at low production cost.

Realistically modeling and rendering the surface characteristics of objects is one of the fundamental aims in computer graphics and computer vision (CG&CV). As a result of remarkable developments in graphical hardware, large-capacity

hard disks, memory devices and networks for computing, storing and transferring heavy image data, it is possible to closely reproduce the shapes and surface characteristics of real objects on a computer, using synthetic images or images of real objects. This technology is capable of having the rapid spread of various applications, such as digital preservation, online exhibition, virtual reality and augmented reality (VR&AR), and object recognition.

1.2. Reflection Properties

Physics of Reflection Properties Surface characteristics of various materials, which include reflection properties, transparency and texture, are essential to distinguish one object from another, and are observable mainly because of interactions between material and illumination. When light strikes the surface of an object, some of it is reflected and the remainder penetrates into the subsurface. The latter may then be absorbed as it travels through the medium, or be transmitted through the subsurface, partially or entirely, if the material is translucent or transparent. Usually, a combination of reflection, transmission, and absorption occurs, and the proportions of light that are reflected, absorbed, and transmitted must sum to one [1, 2].

In CG&CV, all these effects are considered as a local relationship between incoming and reflected light at a surface patch. Theoretically, this relationship can be modeled by the bidirectional reflectance distribution function (BRDF), which is symmetric in the incoming and outgoing directions; this is known as the Helmholtz reciprocity principle. For opaque dielectric materials, the intensity of the reflected light is determined by the light directly reflected at the interface between air and the object's surface, and the light re-emitted from the surface after penetrating into the subsurface of the object and scattering internally. The former is called specular (also known as interface or surface) reflection; the latter is called diffuse reflection (or body reflection), as shown in Figure 1.1. Specular reflection depends on surface characteristics, illumination and viewing directions, and is related to the gloss of the surface material; diffuse reflection is reflected uniformly in all directions, and is the color of the surface material.

Reflection properties are the appearance of object surfaces, including colors,

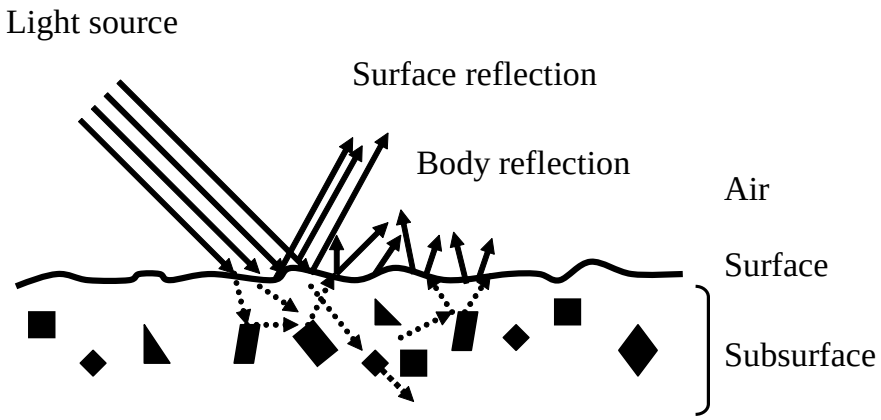

Figure 1.1. Physics of reflected light on surface of dielectric objects

gloss, and surface roughness of the material. Physical color is a function of wavelength, and shows a continuous spectral distribution in the visible range. The spectral distribution is usually integrated into three values such as red, green, blue (RGB) of trichromatic theory, based on human vision and applied to image devices such as a camera. For example, green color is a spectral distribution in the visible range as shown in Figure 1.2, while it is represented as [0, 255, 0] in RGB.

Gloss is a fundamental attribute of an object. The gloss intensity is dependent on illumination and viewing directions, and on the roughness of surface materials of the object. The gloss of an object can be observed by varying the target object, by varying positions of a camera around the object, or by varying illumination directions around the object, as shown in Figure 1.3.

As well as colors and gloss of surface materials, surface roughness is an important factor in characterizing reflection properties. If the surface imperfections are much smaller than the wavelength of incident light, the material is considered optically smooth. In contrast, for rough surfaces, the wavelength of incident light is assumed to be much smaller than the surface irregularities. At a perfectly smooth surface such as a mirror, a specular peak occurs in a direction such that the incident and reflection angles are equal; however at a rough surface, there occurs

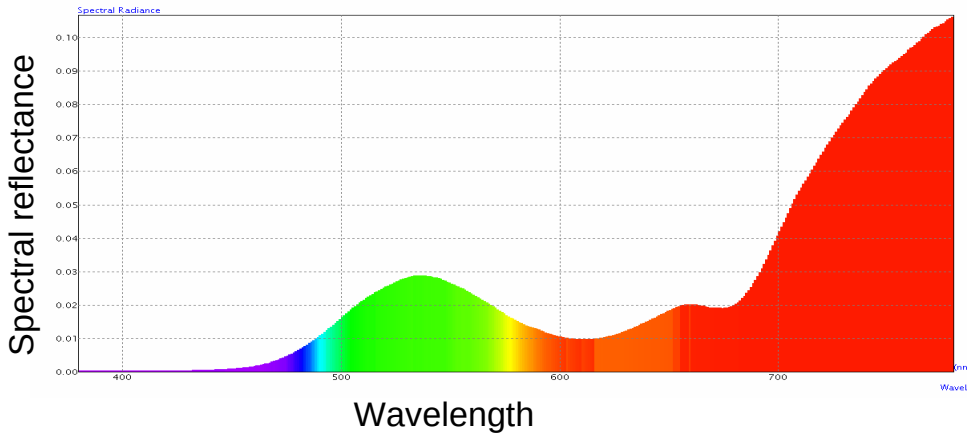

Figure 1.2. Spectral distribution of green color in visible range

Figure 1.3. Gloss of an object varying with different illumination and viewing directions

an angular envelope of specular reflection around the direction of the specular peak, and as the surface roughness and incidence angle increase, a larger-angled envelope is observed.

Surface roughness is often expressed as texture in the CG&CV literature, defined as a visual and tactile quality of an unrefined surface. In early techniques such as texture-mapping, texture segmentation and texture recognition, texture includes both spatial variations (bumps, wrinkles, etc.) on rough surfaces and albedo or color variations on smooth surfaces. Recently, however, as shown in 3D texturing algorithms, texture is emphasized as spatial variations on a rough surface [3].

Techniques of Rendering Reflection Properties Texture mapping is a traditional technique for mapping color and surface details with texture maps or environment maps to a 2D or 3D object model, either computer-

generated or captured using range scanners. This technique is easy and robust for smooth surfaces. For rough surfaces, bump mapping and displacement mapping can produce rich surface characteristics using a heightmap of perturbed surface normal, and relief texture mapping can create 3D surface effects, such as self-occlusion of a surface patch, by augmenting textures with texel depth. In addition, 3D texturing techniques, such as for solid texturing, synthesize and render simultaneously a homogeneous volumetric texture of various refinements by perturbing radial distance [4, 5, 6].

These techniques of model-based rendering, dependent on an accurate geometric model of an object and a single or multiple texture images, are applicable with visual satisfaction for only a limited variety of uses. Instead of an explicitly constructed 3D model, techniques of image-based rendering directly use a collection of images acquired from real objects in particular viewing and illumination directions, based on interpolation or pixel reprojection from source images onto target images. The degree of realism in the synthesized images depends primarily on the quality and quantity of input images, but is independent of surface complexity [7].

In the real world, inhomogeneous object surfaces represent various color appearances in different illuminations, gloss and roughness variations with changing viewing and illumination directions. Using the techniques described above, the mapped textures may be unacceptable in illuminations of a computer-generated environment, especially when specular reflection is present.

To solve the problem of inconsistent optical effects, one approach is to render reflection properties using either numerous BRDF images generated by performing simulations [8, 9, 10], or measured real objects in arbitrary illumination and viewing directions [11, 12]. The other approach is to estimate reflectance parameters from images of real objects based on reflection models [13, 14, 15, 16, 17]. The techniques in either of these two approaches yield efficient results, which are described in more detail in Chapter 3.

Problems with Existing Techniques The methods used to reproduce reflection properties of real objects all depend on the quality of input images, which are captured by an imaging detector such as a camera. However, most commercial cameras are based on RGB trichromatic theory, which transforms

the spectral distribution of physical color into RGB primaries with three-channel filters. The images captured by these cameras may be inadequate representations of the spectral distribution of the reflected light because of factors such as metameric match.

Several methods have been developed to obtain intrinsic information about surface materials and light sources using multispectral information that is transformed from generated or captured RGB values [18, 19, 20, 21, 22, 23, 24, 25], or from images captured by a multiband camera [26, 27]. Since a physical color is a continuous spectral distribution over the visible region, however, converting a small number of primaries into a full spectral distribution of physical color is theoretically an undeterminable function with infinite solutions. A few other methods have been described to obtain images by a spectrograph [28, 29, 30, 31] for material recognition and color reproduction of objects. The images from a spectrograph are captured with a spectral distribution of color at a point or a line on the surface of an object.

Another problem with input images is that since, in the real world, inhomogeneous materials such as ceramic and plastic usually represent a hybrid visual appearance of various colors and gloss, weak or strong, and since normal cameras have a limited dynamic range, acquired images are often too dark in some areas and too bright in others. For a strong glossy area, such as highlights at object surfaces, image values may be clipped to an output limit in the imaging system. For example, values of higher intensity are clipped to gray value 255 for an 8-bit camera, while the information about colors and textures in these areas is lost. However, if the color information behind a strong gloss is obtained by controlling the intensity of illumination, information about colors and textures will be insufficient in dark areas.

Up to now, most studies have assumed that the obtained images are not saturated, and several have focused on obtaining a desired response function by capturing images under different exposure times or shutter speeds, and reconstructing high dynamic range (HDR) images as input images [26, 32, 33, 34, 35, 36]. These techniques are efficient in a case in which the raw images of real objects with gloss are actually unsaturated. However, it is generally difficult to determine the number of raw images and exposure values required for a desired dynamic range

and an effective response function, and the associated computing and storage costs are expensive, since each HDR image is synthesized from multiple images, such as 18 images in [35].

In response to the aforementioned problems with existing techniques, a method has been described to estimate accurate reflectance parameters from spectral images, which are captured with an imaging spectrograph, allowing estimation of the reflectance parameters at each wavelength at a single surface point of real objects [37]. Another method has been introduced to adequately estimate specular reflectance parameters for gloss intensity and surface roughness, even from saturated spectral images, by subjecting only the values obtained at illumination positions where the values are unsaturated to the least squares method [38, 39, 40].

1.3. Realism in CG&CV

Computer graphics (CG) focuses on visual computing, where images are synthesized on a computer using given information about objects (e.g., geometry, reflection properties, illumination), or using altered visual and spatial information sampled from real objects. On the other hand, computer vision (CV) is concerned with theory and technology for building artificial systems by extracting information about objects (e.g., geometry, reflection properties) from one image or a sequence of images of real objects. These two fields have been merged in recent years in simulating or rendering real objects to a synthetic environment, as shown in Figure 1.4.

Creating realistic graphics is the ultimate aim in CG&CV. However, what criteria to use to define realism in images is a controversial problem. Up to now, physical accuracy, perceptual realism, and functional criteria have been applied conceptually to evaluate productions in this field [41, 42].

The criterion for physical accuracy is that the production provides physically intrinsic information. Under this criterion, a synthetic image should be an accurate spectral representation of the values calculated at a particular viewpoint, associated with accurate information about the shapes and material properties of objects and illumination in the scene. In addition, the display device should be able to reproduce accurately an image incorporating all these properties.

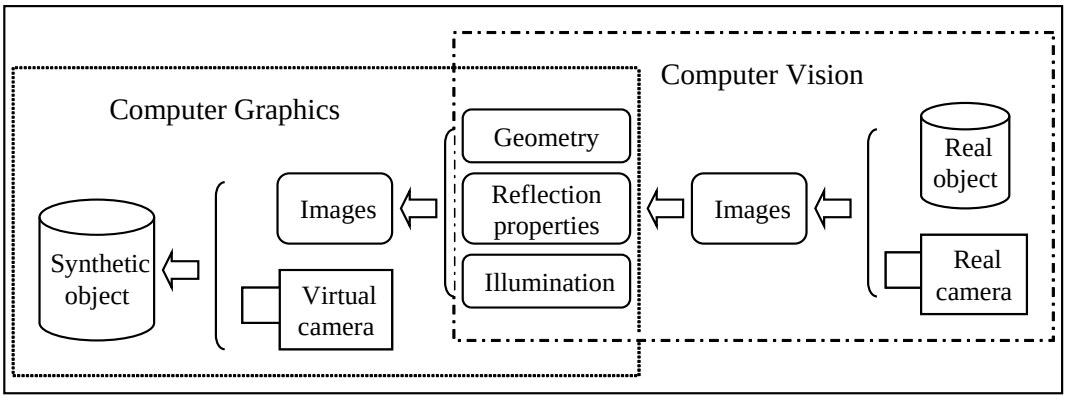

Figure 1.4. Computing process in Computer Graphics & Computer Vision

The physical color of object surfaces is a result of interactions between surface materials and light effects, including absorption and reflection at different wavelengths, and represents a continuous spectral distribution in the visible wavelength range. The spectral radiance $E(\lambda)$ to a camera is affected by the spectral power distribution $L(\lambda)$ of the illumination, the spectral reflectance $O(\lambda)$ of the surface, and by camera sensitivity $S(\lambda)$, as shown in Equation 1.1:

$$E(\lambda) = O(\lambda)L(\lambda)S(\lambda). \tag{1.1}$$

To obtain intrinsic spectral reflectance $O(\lambda)$ of surfaces, it is necessary to remove the spectral radiance of illumination $L(\lambda)$ and camera sensitivity $S(\lambda)$, using an object with a given spectral reflectance.

Reproducing physically realistic images is currently difficult because of the limited quality of existing display devices, and insufficient knowledge about the human visual system; however, it is important to develop physically based methods that are able to obtain accurate information from the measured images of real objects, and to simulate synthetic images with this accurate information.

Photo-realism, another expression for perceptual realism in CG&CV, specifies that a synthetic image should be photometrically realistic, by taking into account the observer's visual properties in the image generation process. Instead of describing the full spectral distribution of colors, current color imaging technology for cameras or display devices is based on trichromatic theory. Using this visually

based technology, different spectral distributions of colors may be integrated into equivalent RGB or other three-channel variables, and existing display devices often cannot reproduce the vast range of strong gloss such as highlights because of their limited dynamic range. However, the standard of photo-realism is sufficient to allow an observer to predict visual appearance with accurate information by applying techniques such as tone-reproduction.

The functional criterion is that the synthetic image should be sufficiently realistic under particular conditions or for particular needs. The fidelity of information that an image provides allows an observer to make reliable visual judgments, and to perform particular tasks according to the visual information, as (s)he does in the real world. In training simulators for sports, driving, or flight, for example, synthetic images are sufficient to allow users to improve their skills by simulating actions in the real world. For online shopping as well, images with high fidelity, generated based on accurate information about real objects, are in demand for successful sales promotions and for minimizing merchandise complaints.

What is described above shows that there are diverse potential rendering styles to produce images with reliable information for an observer. Which criteria to apply for productions in CG&CV depends on the particular requirements. For scientific simulations, it is usually essential to visualize physically accurate information; for entertainment such as games or films, photo-realistic images are often more acceptable. For preservation of cultural heritage artifacts, the primary goal is to record accurate information about real objects, and to display synthetic images based on that information with high fidelity on a computer. Fidelity can be a key criterion to predict synthetic images by perceiving true information in them. However, it is currently difficult to evaluate the relationships among physical accuracy, high fidelity and visual quality. This task requires more multidisciplinary accomplishments in the fields of human vision, computer/machine vision, and visual psychophysics [43].

1.4. Objectives

To record accurate reflection properties of real objects, such as cultural heritage artifacts and commercial items for online shopping, and to exhibit them as syn-

thetic images on a computer, two key points are necessary to take into account:

(i) Obtain accurate reflection properties, including spectral distributions of colors, gloss intensity, and surface roughness of real objects, with the least possible influence of illumination and camera properties used for measurement;

(ii) Reproduce reflection properties faithfully in illuminations of virtual environments such as virtual museums, associated with the shape of objects, as they would be observed in the real world.

The objective of this research is to satisfy these two points. For requirement (i), spectral images, which capture reflected light as a continuous spectral distribution, enable us to provide an adequate record of the reflection properties at object surfaces. Since specular reflection at the surfaces of inhomogeneous objects varies with illumination and viewing directions, as well as with the surface roughness and shapes of objects, it is necessary to rotate light sources or image detectors around target objects, and to revolve the target objects so as to measure reflection properties with the slightest influence of occlusions, shadows, or shade, which may occur between surfaces and between surface patches of the target objects. Next, spectral power distribution of illuminations and properties of image detectors at the point of measurement are removed using a standard whiteboard with a given diffuse reflectance at each wavelength. Reflectance parameters, including diffuse reflectance parameters for colors, and specular reflectance parameters for gloss intensity and for surface roughness, are then estimated accurately at each wavelength and at each surface point of an object from the spectral images, captured with various gradient orientations of the object.

On the other hand, for the second requirement (ii), synthetic images of real objects are reproduced based on the accurately estimated reflectance parameters, with 3D geometric information about the objects, which can be acquired by a range finder or similar instrument. Since the reflectance parameters are estimated with no influence of illuminations and image detectors, it is convenient to multiply the spectral power distribution of illuminations from particular viewpoints in a virtual environment, using Equation 1.1. At the same time, virtual objects can be recreated on a computer with high fidelity by taking into account human color

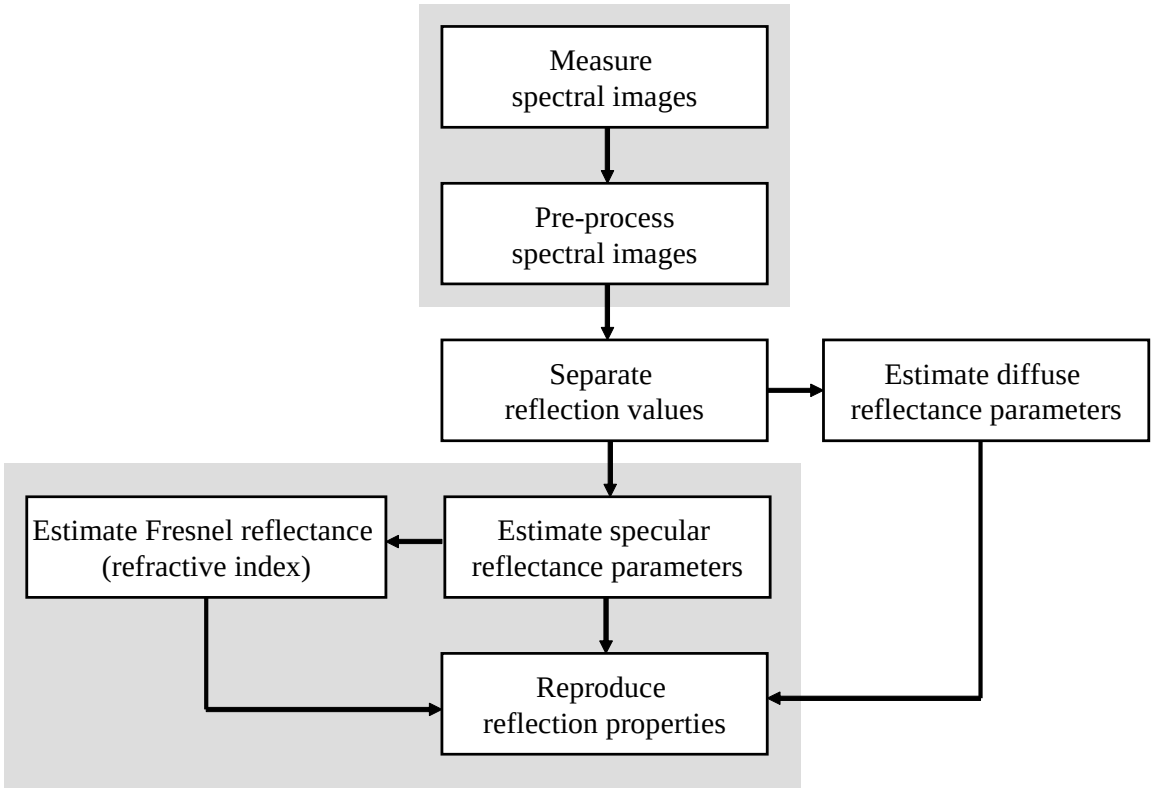

Figure 1.5. Flowchart of present research

perception and the properties of display devices in the image generation process. Furthermore, specular reflection can be synthesized with illumination and viewing directions, associated with the shapes of objects, as it occurs in the real world, by tracking an observer's viewing movement in real time.

Overview of the Dissertation In this dissertation, two methods are described to accurately estimate reflectance parameters using spectral images, and to improve estimation of specular reflectance parameters from saturated spectral images. The flowchart of the present research is shown in Figure 1.5.

A measurement system is constructed with a light source, rotating around a target object between -90^o and 90^o, and an imaging spectrograph equipped with a monochrome charge coupled device (CCD) camera and an objective lens, which is fixed in front of the target object. Since the imaging spectrograph is a line-scanner, the target object is placed on a turntable rotating through 360^o to obtain

spectral images of the whole object. After removing the influence of illuminations and camera properties, spectral images with two axes of wavelengths and spatial positions, captured at different incident positions, are transformed into spectral images with axes of wavelengths and incident positions. Reflection values at each wavelength are separated into diffuse and specular reflection components based on the dichromatic reflection model [44] and the Lambertian reflection model [45], while the diffuse reflectance parameters are estimated during the separation process.

For unsaturated spectral images, the separated specular reflection components are subjected directly to the Torrance-Sparrow reflection model [46, 47], and then specular reflectance parameters for gloss intensity and surface roughness are estimated. On the other hand, for saturated spectral images, after logarithmically transforming the equation of Gaussian distribution in the Torrance-Sparrow reflection model into a linear form, the least squares method is applied to values of the specular reflection components, which are obtained at positions of the light source where the spectral images are unsaturated.

Finally, images are synthesized using the reflectance parameters estimated from spectral images of real objects, associated with several different illuminations separately in a virtual environment, and by taking into account the limited dynamic range of the existing display for strong gloss on the objects' surfaces.

The remainder of this dissertation is divided into six chapters. In Chapter 2, factors influencing reflection properties are described in detail because illumination, camera, and material properties affect measurement of the reflection properties of real objects, reflection models have a great effect on estimating reflectance parameters, and display devices influence the visual appearance of synthetic images. Chapter 3 surveys related work on the techniques of rendering reflection properties, of estimating specular reflectance parameters and Fresnel reflectance, and of measuring spectral images. In Chapters 4 and 5, a measurement system for capturing spectral images and a method to separate reflection components are introduced, respectively. Experimental results, demonstrating that during the separation, diffuse reflectance parameters are estimated at each wavelength, are also presented with discussion in Chapter 5. A method to estimate specular reflectance parameters with and without estimation of refractive index is

described separately; experimental results with synthetic data and measured data are shown, with discussion, in Chapter 6. Chapter 7 gives discussion in correspondence to the assumptions for the whole research, and Chapter 8 summarizes the current work and discusses several possible subjects for future work.

Chapter 2

Factors Influencing Reflection Properties

Light reflected at the surface of an object can be captured into an image by optical devices such as cameras, mirrors, and telescopes, or by natural sensors such as human eyes. Therefore, to obtain an image, a light source, a subject, and an image detector are necessary (a light source can be a subject at the same time), as shown in Figure 2.1. Pixel values in this image are then analyzed with reflection models, and finally the image, either measured or generated, is displayed on a device.

A light source is defined as anything that internally generates and emits light independent of the environment. In general, the radiance from a light source is usually assumed to be constant in each direction, although the geometry of the source such as a point source, line source, or area source may have large effects on the spatial variation of light arriving at the objects around it. Whether the surface of an object looks bright or dark depends on local surface characteristics, on surface orientation, and on spectral power distribution of illuminations. How much light can be captured by an image detector depends on the local surface characteristics, spectral transmission properties of the objective lens with which the detector is equipped, and the spectral sensitivity properties of the detector. More description about illuminations, material characteristics, and image detectors is given separately in Section 2.1, Section 2.2, and Section 2.3.

Representation of an image measured by a camera, or generated analytically

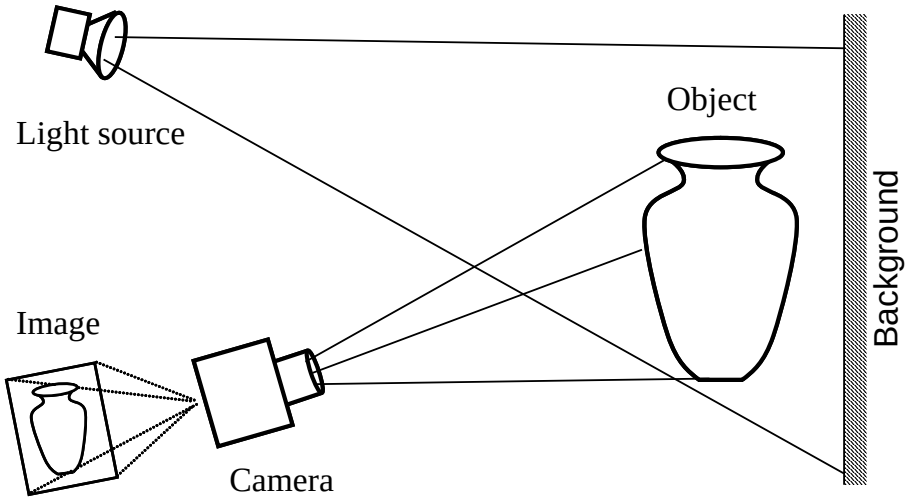

Figure 2.1. Factors in acquiring an image

on a computer, may be greatly influenced by the display devices, as introduced in Section 2.4. Reflection models are important for interpreting pixel values in an obtained image, and to extract object information from the pixel values. In Section 2.5, several reflection models are described in detail.

2.1. Spectral Power Distribution of Illumination

Illuminations, either artificial light sources or daylight, play a significant role in the appearance of object surfaces. Generally, it is assumed that the surfaces of objects do not generate light internally and light sources are treated separately; and that all light leaving a surface at a given wavelength is due to light arriving at the same wavelength. Therefore, light arriving at a surface patch from multiple sources is a linear combination of light from each source, and the proportion from each source depends on the distance and incident angle of the source with respect to the surface patch.

Different illumination has different spectral power distribution, which can be considered as spectral quantities at each wavelength interval. Reflection properties of objects vary in different illuminations, since the intensities and the incident angles of illuminations cause different appearances of gloss and surface roughness,

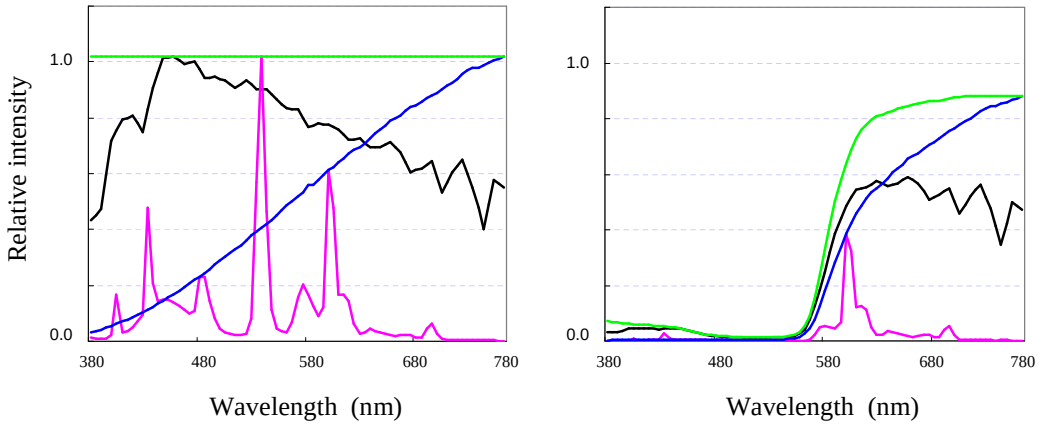

Figure 2.2. (Left) Spectral power distribution of several light sources: ideal white light (red), D-65 (black), halogen light (blue), and fluorescent light (magenta); (Right) Variations in spectral distribution of red color separately under those illuminations

and the reflected light is observed as a product of the spectral power distribution of illuminations and the spectral reflectance of objects at each wavelength, as calculated in Equation 2.1. $E(\lambda)$, $O(\lambda)$ and $L(\lambda)$ are defined as in Equation 1.1.

$$E(\lambda) = O(\lambda)L(\lambda). \tag{2.1}$$

Spectral power distribution of unknown illuminations can be measured, or estimated from images of an object with given spectral reflectance, or estimated from images of several colored objects. Spectral power distributions of several light sources (ideal white light, mimic daylight (D-65), halogen light, and fluorescent light), which are commonly used for experiments in the laboratory, are shown in Figure 2.2 (left), and variations in the spectral distribution of red color separately in these illuminations are shown in Figure 2.2 (right). Clearly, to obtain the intrinsic spectral reflectance of objects, it is necessary to remove the influence of spectral power distribution of the illuminations used for measurement.

2.2. Material Characteristics

Reflection properties at the surface of an object, when the surface is fixed in front of an observer/camera, depend both on the physical characteristics of the surface materials, e.g., metal or dielectric, opaque or translucent, and on the geometric characteristics of the surface.

For a metal surface, only single or multiple specular reflections occur at the interface between the surface and air, and diffuse reflection is often negligible, since the light that penetrates into the subsurface is completely absorbed. Specular reflection is determined by the spectral power distribution of illuminations and the reflectance of the metal, which are variable within the visible spectra. On the other hand, for a dielectric surface, the light partly penetrates into the subsurface and scatters internally, then emits back diffusely out of the surface dependent on spectral reflectance of the surface materials; the remainder of the light is reflected at the interface, often with large effects of the spectral power distribution of illuminations.

According to the scale at which object surfaces need to be described, three different levels of scales are defined to classify the geometric characteristics of object surfaces: macrostructure, mesostructure and microstructure. The macrostructure represents explicit surface features such as polygonal patches, the mesostructure shows small but individually visible geometric details, such as bumps and dents on an orange skin, and the microstructure involves visually indistinguishable surface microfacets, as shown in Figure 2.3.

A surface can either be considered as a collection of patches, with each polygonal patch consisting of multiple microfacets, or it can be assumed to be a collection of microfacets. Reflection properties are closely related to the geometric distribution of these microfacets on object surfaces, since they cause spectral and quantitative variations of the light traveling into and reflecting back out of the subsurface with respect to the wavelength of the incident light. Thus, the intensity and the directions of diffuse and specular reflection at a rough surface vary distinguishably, compared with those at a smooth surface [47, 48, 49].

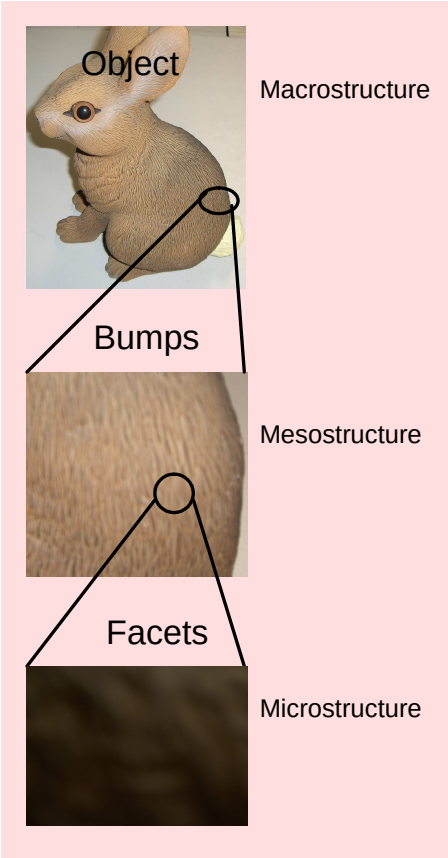

Figure 2.3. Geometric classification of object surfaces

2.3. Properties of Light Detectors

Reflection properties are measured according to the properties of image detectors, including human eyes and cameras. The signal that image detectors record at a surface point of an object may be represented by a single value on a black-and-white camera, by a few values on color cameras, by many values on hyperspectral sensors, or as a continuous function of wavelength on spectrometers.

Spectrometers A spectrometer is an optical instrument to measure the properties of light, such as spectral reflectance and spectral radiance, over a specific range of the spectrum from gamma rays to the far infrared. Spectrometers split incoming light with a prism or a diffraction grating into its component wavelengths, and convert the resulting spectrum to an electrical signal on a photo

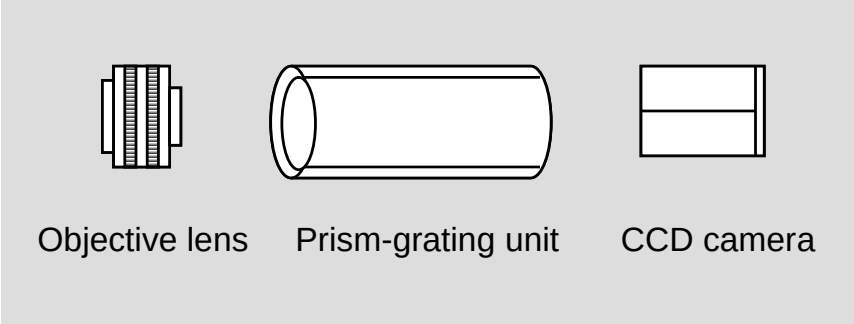

Figure 2.4. A spectrograph

tube or a detector.

Prisms are polyhedral translucent glass or crystal. The spectrum at long wavelengths is refracted less than at short wavelengths when light passes through air and the prism, since the refractive index is dependent on the wavelength of the incident light. On the other hand, the incident light at diffraction gratings is dispersed in multiple directions dependent on the difference of light path length or phase difference between two neighboring gratings. A reflecting plane is adjusted for diffraction gratings to have a suitable angle, and to obtain a strong spectrum in sequential order while avoiding specular diffraction. The spectral resolution of gratings is higher than that of prisms, as a result they are often used in astronomical telescopes.

A spectrograph, as shown in Figure 2.4, measures light reflected at an object as a function of wavelength, based on the same principle as a spectrometer. Light enters the spectrograph through an objective lens, and hits a diffraction grating or a prism through an aperture or a slit on the prism-grating unit. The dispersed light is then focused onto a detector such as a CCD device, and recorded electronically as photographic spectra with respect to wavelengths in an image. The typical spectral resolution of a spectrograph is around 0.2 nm [50]. However, the resolution of measurement ultimately depends on the properties of the CCD device.

Human Perception The human eye is an exquisite optical device that focuses an image on a light-sensitive surface by means of the main elements of the eye. The iris and the pupil control the amount of light penetrating the eyeball;

the cornea and the crystalline lens refract the light to create a retinal image on the retina. The pupil, whose diameter ranges from about 1 to 8 mm, can respond to illumination changes with a ratio of about 28 to 1. The retina consists of two types of photoreceptors, rods and cones, which respond to light in the wavelength range between 330 nm and 810 nm. Rods provide achromatic vision at scotopic levels within the range of 10^{-6} to 10 cd/m^2; and cones play roles within the range of 0.01 to 10^8 cd/m^2. Both rods and cones function in the overlap between 0.01 and 10 cd/m^2. Thus, human eyes can have a dynamic range of illuminance of more than 10 million to 1, from full sunlight to starlight [31].

Cones on the retinal cells produce the sensation of color. The genetics of color vision has revealed that the cones of human eyes for most observers comprise three types of receptors with sensitivity peaks in short, medium, and long wavelength light (called S cones, M cones, and L cones, respectively). The response of a receptor to incoming light can be obtained by summing the product of the sensitivity and the spectral radiance of the light over all wavelengths, as shown in Equation 2.2:

$$R_k = \int_\Lambda S_k(\lambda)L(\lambda)d\lambda, \tag{2.2}$$

where R_k and S_k represent the response of the kth type of receptor (S, M, or L), and its sensitivity; $L(\lambda)$ is the incident radiance at the receptor; and Λ is the range of visible wavelengths.

Since human eyes have three types of color receptors that respond to different ranges of wavelengths, a set of standard primaries and three values of weights to describe light using those primaries are obtained by performing color matching experiments. The spectral radiance of a light source can be considered as a weighted sum of three channel quantities using the primaries R, G, and B, and each of the weighted values with respect to the primaries can be considered as the response to the light source over all wavelengths. This process can be written as

$$\begin{aligned} L(\lambda) &= \omega_1 R + \omega_2 G + \omega_3 B, \\ &= \Big\{ \int_\Lambda r(\lambda)L(\lambda)d(\lambda) \Big\} R + \Big\{ \int_\Lambda g(\lambda)L(\lambda)d(\lambda) \Big\} G + \Big\{ \int_\Lambda b(\lambda)L(\lambda)d(\lambda) \Big\} B, \end{aligned}$$

where $L(\lambda)$ is the spectral power distribution of a light source, and ω_1, ω_2, and ω_3 are a set of weighted values. $r(\lambda)$, $g(\lambda)$, and $b(\lambda)$ are color matching functions with respect to primaries R, G, and B, respectively [2, 51].

The process to convert a given spectral power distribution to its corresponding RGB color values is straightforward; however, the reverse transformation is not a unique operation. There are infinitely many spectra corresponding to a given RGB triplet. Therefore, based on the trichromatic theory, equivalent three-variable triplets such as RGB are given for a particular observer/camera or in a particular condition (illumination, viewing angle, etc.), although the spectral power distributions are different. This phenomenon of metamerism causes difficulties for reproducing original colors, which are inherently determined by the spectral distribution of light.

Image Devices An image is the light energy that is transformed into electronic signals by image devices. An image device may measure an area, a line, or a point on the surface of an object. Although most commercial image devices use area sensors, high resolution can be obtained by line-scanning devices, at much lower cost than point devices. Here, CCD cameras and lenses are described in detail.

A CCD is an image sensor that contains an array of coupled metal-oxide semiconductor (MOS) capacitors sensitive to light. Electric charges accumulate on the capacitor array when an image is projected through a lens. For digital color cameras, there are two ways to separate colors: the common one is to use a Bayer mask over the CCD, on which green elements are twice as numerous as red or blue; the other way is to use three CCD devices and a dichroic beam splitter prism, which splits the image into red, green and blue components.

With black-and-white CCD cameras, the sensor response I_p at a surface point p can be modeled as

$$I_p = \int_\Lambda L(\lambda) O_p(\lambda) S(\lambda) d\lambda, \tag{2.3}$$

where $O_p(\lambda)$ is the spectral reflectance of the surface material at p, and $S(\lambda)$ is the sensitivity of the device with respect to the wavelength. With color cameras,

the sensor response can be considered as that at each color channel separately, while taking account of the effect of the associated filter response.

There are several physical phenomena that affect the ideal response of CCD cameras, especially for color signals:

1. Clipping. Input signals are clipped whenever the accumulated signal exceeds the highest processable voltage. For a usual 8-bit gray-scale analog/digital converter (ADC), the clipping threshold may be 255 (or 1.0). Clipping at different channels for color cameras may cause hue and saturation distortion varying with intensity of the incident light at the CCD chip.

2. Blooming. When the incoming light signal at a CCD cell exceeds the clipping threshold, the extra charge spreads into the neighboring CCD cells. As a result, information at the affected pixels in an image may be inaccurate due to this blooming effect.

To improve the dynamic range of a camera, there are two approaches: reduce current dark noise by cooling the CCD device, or synthesize an HDR image with the raw images measured at different exposure times or shutter speeds.

Other factors, such as fabrication defects and quantization noise, are appropriately compensated by simple statistical models, e.g., a Poisson-distributed random variable for the CCD bias, or a random integer variable for dark current [2, 51, 52].

As well as CCD chips, image sensors composed of complementary metal-oxide semiconductor (CMOS) chips have recently been developed with improved high noise immunity, high speed process, and low static power consumption. Because of these advantages of CMOS sensors, CMOS processes have comprised the vast majority of integrated circuit manufacturing in recent years. However, CCD sensors are still widely used because they possess a higher sensitivity and a higher dynamic range than CMOS sensors can provide.

Lenses are positioned in front of the opening of most optical sensors to gather the incoming light and to focus an image on the device. Since the materials used for lenses are transparent, light going through the lenses is refracted according to Snell's law, as shown in Equation 2.4:

$$n_1(\lambda)\sin\alpha_1 = n_2(\lambda)\sin\alpha_2, \tag{2.4}$$

where n_1 and n_2 are the refractive indices of the first and second medium at each wavelength λ, respectively; α_1 is the incident angle; and α_2 is the refractive angle. The reflection effects at the surface of a lens can be ignored by assuming that the angles between the incident light and the refracting surfaces of the lens are small.

To obtain an image with proper contrast between bright and dark areas at an object surface, the incident light to the lens can be controlled by adjusting the aperture diameter of the lens using an iris diaphragm, or by manually or automatically adjusting exposure time with a shutter over the lens [2, 51].

2.4. Properties of Display Devices

Synthetic or measured images have to be displayed on a photo film or an electronic device, and go through the filter of human visual perception. Displays are electronic devices to represent images in visual or tactile form. Colors on a given display device are specified using an index into a hardware color palette, or using an RGB triplet. Images are usually produced with a camera, or on a computer using input RGB data or spectral data, in a 24-bit or 32-bit RGB space with 8 bits allotted to each of the three primaries and depth.

Most display devices perform poorly for high contrast images with both dark and bright areas, which may contain contrasts as large as 100,000:1 or more. Unlike the dynamic range of the human vision system, the intensity of a typical cathode-ray tube (CRT) display spans from 1 to 100 cd/m_2. Liquid crystal displays (LCDs) generally have an even lower dynamic range than CRT displays because of the backlight lamp. Emissive displays, where all pixels emit light individually, such as plasma displays, the latest organic light-emitting diode (OLED) displays, or surface-conduction electron-emitter displays (SEDs), are theoretically capable of achieving a higher dynamic range than CRT displays, e.g., a dynamic range of 5,000:1, when the input signal spans brightness from 0 to 100% simultaneously.

With the limited dynamic range of commercial display devices, the subtle

textures and original details in images may be inadequately reproduced. Images with high contrast can be displayed on existing devices with perception realism using tone reproduction technology [31, 53, 54].

2.5. Reflection Models

An appropriate reflection model is essential for analyzing captured images and obtaining proper information about objects such as reflection properties, material characteristics and shape information.

Roughly, according to where the light arrives at a surface, reflection models can be classified into two main groups: local reflection models, which assume that the incident light comes only from light sources and proceeds directly to the camera; and global reflection models, which treat the incoming light at a surface patch as a combination of light from sources and from other surfaces, or even from other patches on the same surface. On the other hand, from the viewpoint of the reflection behavior of the light at a surface patch, reflection can be divided into diffuse reflection and specular reflection.

Interreflections, which occur between objects (including ambient illumination), between surfaces, or between surface patches on the same surface, lead to varieties of complex shading effects. Since interreflection effects are still poorly understood, some reflection models ignore these effects by restricting conditions, while others take them into account. In general, the interreflected light at a surface patch, whether the incident light is from other objects or from other surfaces of the same object, and however many times the interreflection occurs at this surface patch, can be incorporated into either diffuse or specular reflection that occurs at the same surface patch.

In this section, several typical reflection models in CG&CV that are used to predict and interpret reflection properties at an object surface are described in detail.

The BRDF model is a basic local reflection model to define the ratio of radiance in the outgoing direction to that in the incident direction, as shown in Figure 2.5.

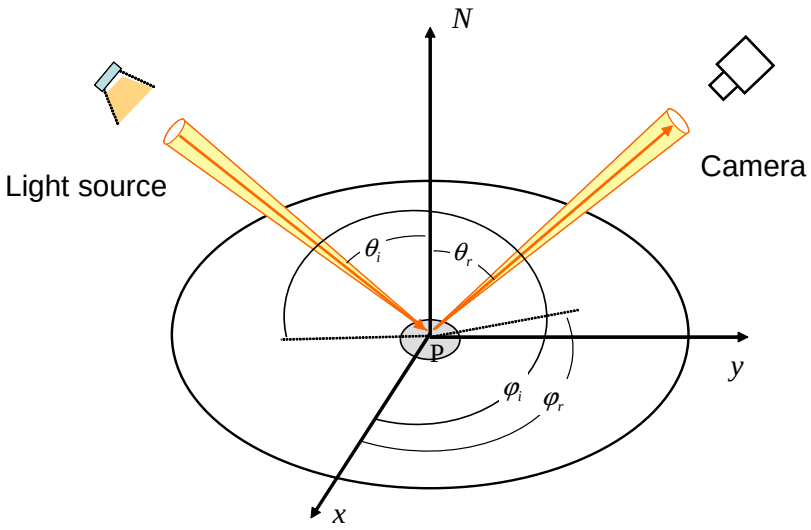

Figure 2.5. BRDF model

From BRDF ρ_{brdf} at a surface patch P, the outgoing radiance $E_P(\lambda, \theta_r, \phi_r)$ at the patch P in (θ_r, ϕ_r) direction can be modeled in the θ, ϕ angular coordinate system on a hypothetical hemisphere of directions centered at P, as shown in Equation 2.5:

$$E_P(\lambda, \theta_r, \phi_r) = \int_{\Omega} \rho_{brdf}(\lambda, \theta_r, \phi_r, \theta_i, \phi_i) L_P(\lambda, \theta_i, \phi_i) \cos\theta_i d\omega, \tag{2.5}$$

where $L_P(\lambda, \theta_i, \phi_i) \cos\theta_i d\omega$ represents incoming radiance from a solid angle $d\omega$ in (θ_i, ϕ_i) direction, and Ω represents the hemisphere of illumination. The BRDF model is physically accurate, and covers anisotropic and isotropic reflections. However, BRDF measurements are difficult practically and expensive for a large number of combinations of illumination and viewing directions, especially for objects with complex shapes and surface features.

The Lambertian reflection model [45] is widely used in CG&CV to model radiance reflected at a Lambertian surface, which is proportional to the cosine of the incident angle. BRDF at Lambertian surfaces is independent of reflected directions. In this case, the reflected radiance $E_d(\lambda)$ and the BRDF ρ_{brdf} are constant. Diffuse reflectance (also known as albedo) R_d for a Lambertian

surface is defined as the fraction of the incident irradiance that is reflected at the surface in all directions, as a value range [0,1]. The radiance reflected at a surface can be represented by Equation 2.6 as

$$E_d(\lambda) = \int_{\Omega} R_d(\lambda) L(\lambda) \cos\theta_i. \tag{2.6}$$

For rough diffuse surfaces such as clays and sands, and for smooth diffuse surfaces, generalized Lambertian models are developed empirically or theoretically, by taking account of geometric effects between surface microfacets for directional diffuse reflection, or of individual subsurface inhomogeneities for Fresnel-corrected diffuse reflection [55, 56].

The Torrance-Sparrow reflection model [46, 47], based on geometric optics, is a simpler model for specular reflection than the Beckmann-Spizzichino model [57], which is based on physical optics. Both of these models are considered theoretically more accurate than the empirical Phong reflection model [58]. Relative to the surface roughness, specular reflection involves a specular spike, which occurs at a mirror-like surface or in the mirror-like direction $\theta_i = \theta_r$ at a rough surface, and a specular lobe, which is symmetric with respect to the mirror-like direction.

The Torrance-Sparrow model assumes that surface roughness is greater than the wavelength of the incident radiance, and that surfaces are a collection of planar, perfectly specular reflecting microfacets, as shown in Figure 2.6. The surface has a mean normal vector N, and the normal vectors of each microfacet in the surface, which deviate normally from the mean normal N by angle α, can be modeled as a mathematical function of Gaussian distribution with standard deviation σ.

This reflection model, as shown in Figure 2.7, describes the fraction of incident light that is reflected at a microfacet with the Fresnel reflectance $F(n(\lambda), \theta_i)$, and considers masking and shadowing between microfacets on the surface by means of the geometrical attenuation factor G. The reflected radiance at surface patch P is described by Equation 2.7, where R_s represents specular reflectance, and σ represents surface roughness. The rougher the surface, the less intensive specular reflection occurs.

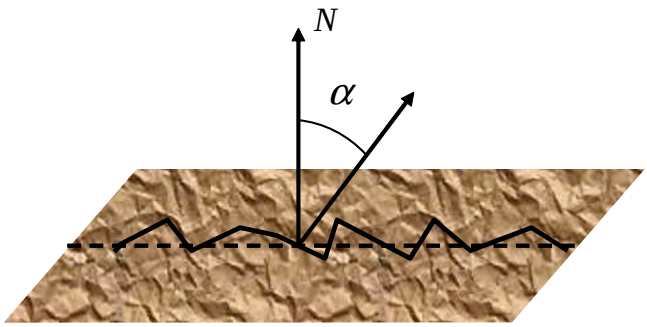

Figure 2.6. Microfacets-based surface in the Torrance-Sparrow reflection model

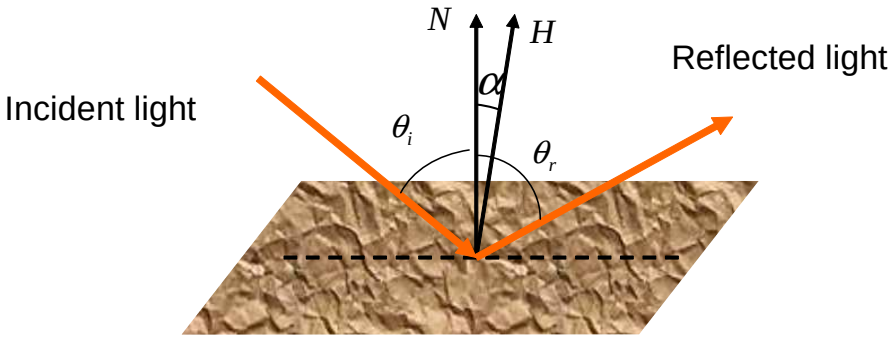

Figure 2.7. Torrance-Sparrow reflection model

$$E_s(\lambda, \theta_r) = F(n(\lambda), \theta_i) G R_s(\lambda) e^{-(\alpha/\sigma)^2} L_P(\lambda) / \cos\theta_r. \tag{2.7}$$

The Fresnel reflectance for unpolarized incident light can be expressed in terms of the refractive index $n(\lambda)$ and the absorption factor a, as shown in Equation 2.8, where $n(\lambda)$ varies with wavelength of incident light; and for the dielectrics, a is usually 0.

$$F(n(\lambda), \theta_i) = \frac{1}{2} \frac{(g(\lambda, \theta_i) - \cos\theta_i)^2}{(g(\lambda, \theta_i) + \cos\theta_i)^2} \left(1 + \frac{(\cos\theta_i (g(\lambda, \theta_i) + \cos\theta_i) - 1)^2}{(\cos\theta_i (g(\lambda, \theta_i) - \cos\theta_i) + 1)^2}\right), \tag{2.8}$$

where $g(\lambda, \theta_i) = \sqrt{(n(\lambda) - ia)^2 + \cos^2\theta_i - 1}$.

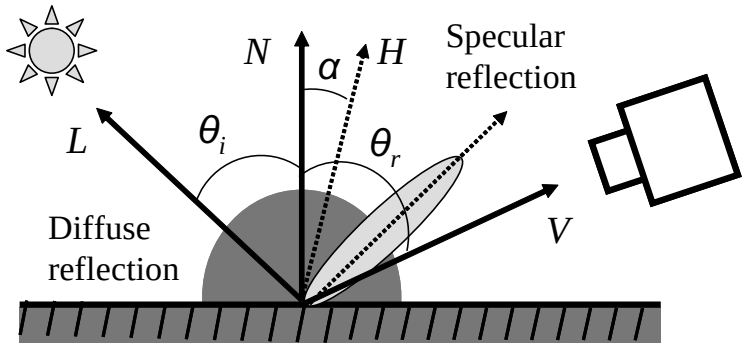

Figure 2.8. Reflections at object surface

By taking the Fresnel reflectance and the geometric attenuation factor into account, the Torrance-Sparrow reflection model is capable of predicting reflections from both metal and dielectric objects with interreflections between surface patches. Generally, in CG&CV, a simplified version of the Torrance-Sparrow model is used to describe the specular reflection component by assuming the Fresnel reflectance and the geometric attenuation factor to be constant [52, 59].

The dichromatic reflection model considers reflections at a surface patch of inhomogeneous dielectric objects as a linear summation of diffuse and specular reflection components, as shown in Figure 2.8, since, in the real world, few surfaces are ideally diffuse or perfectly specular. H is called the half-vector and represents the normalized vector sum between the illumination vector L and the viewing vector V. α is the angle between the normal vector N of the object surface and the half-vector H. The radiance at a surface patch P in a given direction is approximated as shown in Equation 2.9, if applying diffuse and specular reflection to the Lambertian and Torrance-Sparrow reflection models, respectively. Note that for dielectric objects, specular reflection is assumed to be independent of the wavelength of incident radiance [2, 44, 52].

$$E_P(\lambda, \theta_r) = R_d(\lambda) \int_\Omega L_P(\lambda) \cos\theta_i d\omega + R_s(\lambda) F(n(\lambda), \theta_i) G e^{-(\alpha/\sigma)^2} L_P(\lambda) / \cos\theta_r. \tag{2.9}$$

In addition to the reflection models described above, other reflection models have

been developed in CG&CV. The He reflection model, based on physical optics, analytically predicts specular reflection, directional and uniform diffuse reflections at the surface of metal or dielectric objects [60]; the Lafortune reflection model incorporates off-specular reflection and retro-reflection using a Monte Carlo path tracing program [61]; and other reflection models simulate the reflections for anisotropic materials such as brushed metal and finished wood [11, 62, 63].

Chapter 3

Related Work

Reflection properties of object surfaces are essential information for distinguishing one object from another, and for recovering 3D object features such as the material characteristics of object surfaces and surface orientations. There have been a large number of studies in CG&CV to obtain reflection properties of real objects by measurement, and then to reproduce realistic reflection properties as synthetic objects on a computer. Many techniques do not work properly when glossy objects exist, however, especially when specular reflection is saturated, appearing as highlights in the captured images.

In early techniques of model-based and image-based rendering in CG&CV, one of the fundamental problems was optical inconsistency, which occurrs when the illumination directions in a virtual environment are mismatched with the illumination directions in which the input images were captured. To solve this problem, there are two main approaches: one is to model and render reflection properties at object surfaces with BRDF or bidirectional texture function (BTF) images, which is called **BRDF image-based rendering** in this dissertation; the other is to estimate reflectance parameters by subjecting measured images to reflection models, and to reproduce reflection properties of objects associated with illuminations in a VR&AR environment, which here is called **estimating reflectance parameters**. These two approaches are both based on physics and optics relative to light transmission and reflection at the surface of an object.

3.1. BRDF Image-based Rendering

BRDF measurement has mainly been used in the fields of optical engineering and remote sensing, and only since the early 1990s has it become practicable in CG&CV. BRDF data can be simulated using a virtual gonioreflectometer based on the physical theory of BRDF, albeit with expensive computation cost [8, 9, 10].

BRDF images for both isotropic and anisotropic materials are captured using an imaging gonioreflectometer with a fish-eye lens near grazing angles, but without sharp specular reflection, and are applied to a selected analytic model [11, 61]. The CUReT database has been built with BTF measurements of over 200 combinations of illumination and viewing directions for a planar patch of 60 different materials. The samples include smooth and rough surfaces of isotropic and anisotropic materials, and, especially for anisotropic materials, the measurements are carried out by rotating the samples by either 45 degrees or 90 degrees. The BTF images are captured with 640×480 pixels, 8 bits per RGB channel using a 3-CCD video camera, and are averaged over each sample area to obtain the BRDF images [12]. Using BRDF images from the CUReT database as reference images, several techniques have been developed to synthesize and predict reflection properties with 3D textures at the surface of objects in novel illumination and viewing directions [64, 65].

Recently, more robust and practicable BRDF/BTF measurement systems have been described using a second camera attached to the light source for capturing images to calibrate positions of the light source [66], and using a single concave parabolic mirror to control illumination angles over the hemisphere to the surface point and to record reflectance from multiple viewing directions over the hemisphere [67]. The latter measurement system is capable of predicting specular reflection in illumination and viewing directions as a path along with a translating illumination aperture.

The techniques in this approach usually provide rich color and gloss of synthetic objects in VR&AR, while the realism of reflection properties is determined by the quality and quantity of input images of real objects, taken in arbitrary illumination and viewing directions. However, these techniques require large-capacity storage for the raw input images and high-speed processing capability on a computer, and apply previously developed techniques of image-based render-

ing, such as interpolation, which often present difficulties for obtaining physical accuracy of reflection properties with surface variations synthesized in novel illumination and viewing directions.

3.2. Estimating Reflectance Parameters

The approach of estimating reflectance parameters based on reflection models is often more practicable in applications. Basically, reflection at the surface of an inhomogeneous dielectric object is considered as a combination of diffuse and specular reflection components, as shown in Equation 2.9. Several techniques have been developed to simultaneously estimate diffuse reflectance parameters R_d, specular reflectance parameters R_s for gloss intensity, and σ for surface roughness from captured images of real objects using a nonlinear least squares fitting algorithm, with expensive time and computation costs.

Abundant research is available in the literature to separate reflection values into diffuse and specular reflection components on the basis of the dichromatic reflection model, and on the basis of several geometrical or physical differences between diffuse and specular reflections.

First, the light of diffuse and specular reflections has different transmitted radiance, dependent on polarizer orientation. For dielectrics, the diffuse reflection components tend to be unpolarized while the specular reflection components vary as a cosine function with rotation of a polarization filter. Using a polarization filter alone, image values may be separated into diffuse and specular reflection components by pre-segmenting highlight areas with the assumptions that the surface is smooth and with a uniform color [48, 68, 69].

Second, for dielectrics, diffuse and specular reflection components have different spectral distributions. As projected in color space, image values are clustered as a **T**-shape or **L**-shape, with two vectors in different directions (diffuse and specular reflection components) when the surface is smooth, and can be segmented into different color areas. The two reflection components can be separated by segmenting the two vectors in color space using the principal component analysis (PCA) method or the Hough transformation method [13, 17, 70, 71, 72]. Algorithms using both polarization and color information can separate diffuse and

specular reflection components at a textured surface, while taking into account interreflections [14].

Third, an epipolar plane image (EPI) can be acquired by slicing the EPI volume, which is constructed by taking a sequence of regularly spaced images with linear camera motion. The EPI strip-pattern of specular reflection components in a spatio-temporal EPI has a more vertical orientation than that of diffuse reflection components for convex surfaces, and a more horizontal orientation for concave surfaces. Based on the EPI strip-patterns of diffuse and specular reflections, the two reflection components can be separated with geometric and photometric constraints [73, 74].

Fourth, as ideal diffuse reflection follows a cosine function, the light scattered at the surface disperses uniformly in all directions, and the intensity depends on the spectral reflectance of surface materials; while specular reflection can be modeled as the Torrance-Sparrow reflection model based on geometric optics, or as the Beckmann-Spizzichino reflection model based on physical optics, the intensity varies dramatically with the illumination and viewing directions and the surface characteristics. These two reflection components can be separated by picking up the pixels in input images below threshold values, which contain only diffuse reflection components, or by using images taken at the positions of the light source, where only diffuse reflection occurs [13, 15, 16, 75, 76].

Most algorithms for separating diffuse and specular reflection attempt to acquire only diffuse reflection for vision techniques, such as image segmentation and motion detection, by eliminating specular reflection in the input images, since the positions and intensities of specular reflection such as highlights produce erroneous results. Some of the algorithms take advantage of the separated specular reflection components for object recognition, illumination localization, and for recovering the shape or surface curvature of objects.

By applying the separated diffuse reflection components to diffuse reflection models, and applying the separated specular reflection components to specular reflection models, the diffuse reflectance parameters R_d, specular reflectance parameters R_s for gloss intensity, and σ for surface roughness can then be estimated, according to the required objectives and the applications.

3.3. Estimating Specular Reflectance Parameters

There has been much research on synthesizing images with specular reflection using ray tracing or environment mapping, and on reproducing specular reflection of real objects in CG&CV, since specular reflection can be an important cue for realistic images. Early research on specular reflection focused on addressing the issue of gloss perception, and on determining its relations with surface curvature and the shape of objects. Recently, specular reflection, and the interactions with the material characteristics of object surfaces, have become a prominent subject [77, 78].

Most models for specular reflection take into account interactions between intensity of gloss and surface roughness. On the basis of these reflection models and geometric information about real objects, specular reflectance parameters for the intensity and surface roughness can be estimated using a sequence of images captured at positions where specular reflection occurs.

Sato et al. introduced a method using a sequence of range and color images of real objects to estimate reflectance parameters with object shapes [15]. The range images and color images were captured with a light-stripe rangefinder and a 3-CCD camera, which were fixed in front of a target object, while the object was rotated by a robotic arm. First, the object was reconstructed with the range images, and was texture-mapped with the color images. Reflection values were then separated into diffuse and specular reflection components based on the estimated surface normals. Finally, based on the Torrance-Sparrow reflection model, specular reflectance parameters for specular intensity and surface roughness were estimated from the separated specular reflection components, at the selected surface mesh of the reconstructed object, where the intensities of diffuse and specular reflection are both large.

Without using range images, Omata et al. proposed a method to estimate reflectance parameters with object shapes by analyzing intensity changes of image values at each pixel in a sequence of input images with hypothetical rotation of a light source [76]. The images of a target object were measured using a fixed 3-CCD camera and light source, while the target object was rotated on a turntable. Diffuse and specular reflection components were separated by selecting reflection values that only included diffuse reflection components, and diffuse reflectance

parameters and surface normals were then estimated. After correcting surface normals with the maximal value of the separated specular reflection components at each pixel, based on the Phone reflection model, specular reflectance parameters for specular intensity and for surface roughness were estimated by varying the specular parameters for surface roughness between 3 and 300, until the difference between the theoretical and separated specular reflection components was a minimal value.

Machida et al. proposed a method using both range and color images to estimate reflectance parameters with object shapes [79]. The range and color images of a target object were acquired with a 3-CCD camera and a laser rangefinder, which was aligned with multiple (maximum 60) surrounding position-given point light sources. In addition, the camera and rangefinder were both rotated around the target object. The color images were captured only at selected light source positions where the pixels had been observed once for the diffuse only reflection component and twice for strong specular reflection components with respect to the object geometry. By classifying the pixels in color images into two groups of diffuse only reflection and strong specular reflection components, diffuse and specular reflection components were separated. Specular reflectance parameters for specular intensity and surface roughness were estimated based on the Torrance-Sparrow reflection components. A notable point of this method is that it enables interreflections to be taken into account.

Several other techniques using BRDF images captured in arbitrary illumination and viewing directions at glossy rough surfaces have been developed to estimate specular reflectance parameters for specular intensity and for surface roughness at the mesostructure or microstructure level.

Chen et al. described a method to estimate surface mesostructure with specular intensity from BRDF images of complex real objects that are translucent and strong glossy, such as orange skin and jelly candy [49]. The BRDF images were measured densely with a fixed digital camera and a manually moving point light source, and a checkerboard and four specular spheres for geometric calibration and light source estimation. Diffuse and specular reflection components were separated using a histogram thresholds method. From the specular reflection components, the parameters for surface normal and for surface roughness were

then estimated with the peak values at each pixel.

Wang and Dana developed a method to estimate relief texture with specular intensity from BTF/BRDF images [80]. The images were captured point-by-point using a mirror-based imaging device [67], with surface normal simultaneously at each point of glossy object surfaces. After compensating the raw images for the distance between each pixel and the focus point on the mirror, pixels with intensity values greater than a threshold (240) were used to estimate the parameters for surface roughness associated with the surface normals of the pixels.

Another technique was introduced to obtain reflectance parameters by analyzing the space of densely-sampled BRDF images of more than 130 common materials [35]. For each sample material, 20-80 million BRDF images were acquired with a high-resolution camera and a light source, which was mounted on an arm of a turntable, orbiting the target sample. The dimensions in space of all possible BRDF images, generated by interpolating and extrapolating each raw BRDF image as a single high-dimensional vector, were reduced in linear subspace and nonlinear manifold analysis to define model parameters for varieties of materials. The specular intensity and surface roughness of a glossy object surface could be characterized perceptually using the material parameters associated with the illumination and viewing directions, as well as representing other surface characteristics of objects, such as metallic-like and fabric-like.

3.4. Estimating Fresnel Reflectance

A rough surface of an object can be considered as a collection of microfacets, each of which is mirror-like. Specular reflection at the surface can be modeled by describing the distribution of microfacets, with Fresnel reflectance on each of them [46, 47]. With a given refractive index, which is a function of wavelength at the surface patch, the Fresnel reflectance can be computed in Equation 2.8 at different incident angles. However, since the refractive index is determined by the physical characteristics of surface materials, the refractive indices of only limited kinds of common metal and nonmetal materials are currently available in the Handbook of Optics [81], and in cases such as when the surface is stained, the actual indices may be different.

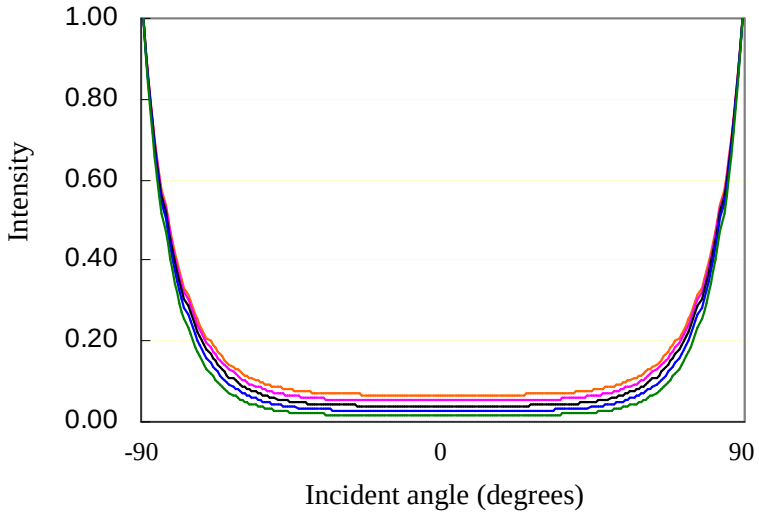

Figure 3.1. Fresnel reflectance at different incident angles, and with the refractive indices range [1.3,1.7], increasing from bottom to top

To confirm that Fresnel reflectance varies with incident angle and wavelength variation of refractive index, the Fresnel reflectance in terms of Equation 2.8 with refractive indices between 1.3 and 1.7, and incident angles at 0.75^o intervals between -90^o and 90^o, are synthesized, as shown in Figure 3.1. The effects of incident angles and refractive indices on Fresnel reflectance are verified: as the incident angles approach $\pi/2$, the Fresnel reflectance approaches 1.0; the larger the reflective index, the larger the Fresnel reflectance. Therefore, it is necessary to estimate the refractive index at each wavelength from reflection properties at surfaces of a real object in some applications [82].

Cook and Torrance introduced a method to estimate refractive index with a given Fresnel reflectance F_0 at normal incidence, where $\theta_i = 0$, using the simplified Equation 3.1 [47]:

$$F_0(\lambda) = \left(\frac{n(\lambda) - 1}{n(\lambda) + 1}\right)^2. \tag{3.1}$$

For a copper surface, values of Fresnel reflectance were calculated corresponding to the normal reflectance, and then used to interpolate between the color of the

material ($\theta_i = 0$) and the color of the illuminations ($\theta_i = \pi/2$) at each channel of R, G, and B. This method ignored the fact that refractive indices and Fresnel reflectance depend on the wavelength of incident light, although the RGB values of material and illumination for synthetic objects were transformed using given spectral reflectance of the material and given spectral power distribution of the illumination.

Tanaka and Tominaga described a method to estimate refractive index for a dielectric object, on the basis of the two assumptions that the refractive index was independent of wavelength and that the specular reflectance parameter for specular intensity was constant near grazing angles [72]. The specular reflection components were separated using the two vectors in RGB color space from the images captured by a monochrome CCD camera with an RGB filter. Surface normals were estimated using an iterative algorithm, with the pixel of peak value of the specular reflection components as the initial value. By varying the refractive indices between 1.3 and 1.7 in Equation 2.8, specular reflectance parameters for specular intensity and for surface roughness were estimated based on the Torrance-Sparrow reflection model, and the refractive index was determined, until the difference between the theoretical and separated specular reflection components was minimal.

3.5. Conclusions

The aforementioned techniques, as partly summarized in Table 3.1, can provide visually rich reflection properties of virtual objects, and some of them can even reproduce the shape of the objects associated with the Fresnel reflectance. However, these techniques all used RGB images of real objects, and rely on the assumption that the input images are unsaturated, by controlling the illumination intensity or by generating HDR images as the input images. With this assumption, the peak intensity of specular reflection components at the normal incidence is available; therefore, the surface normals can be estimated, and the refractive indices can be calculated simply. On the other hand, the present work can estimate accurate reflectance parameters using spectral images, by replacing values that are saturated due to the limited dynamic range of a CCD camera.

Table 3.1. Related work to estimate reflectance parameters

	Object characteristics		Image properties			Estimation of reflectance parameters			
	Object surface	Surface normal	Number of images	Channel of images	Dynamic range	Separation method	Specular reflection	Interreflection	Fresnel reflectance
Klinker 1988 [69]	uniform color	given	single image	RGB (3)	threshold (maximum)	color histograms	estimation of parameters	ignored	ignored
Wolff 1990 [48]	uniform color	given	single image	black/white (1)	ignored	polarizing filter	no estimation	ignored	estimated
Ikeuchi 1991 [74]	uniform color	measured	single image	black/white (1)	ignored	incident positions	estimation of parameters	ignored	constant
Sato 1997 [15]	complicated colors	measured	sequence of images	RGB (3)	ignored	incident positions	estimation of parameters	ignored	ignored
Nayar 1997 [14]	complicated colors	estimated	multiple images	RGB (3)	ignored	polarizing filter, color histograms	no estimation	estimated	estimated
Tanaka 2000 [71]	uniform color	estimated	single image	RGB (3)	ignored	color histograms	estimation of parameters	ignored	estimated
Omata 2000 [75]	color segmentation	estimated	sequence of images	RGB (3)	ignored (12bit)	intensity changes	estimation of parameters	ignored	ignored
Tan 2005 [17]	complicated colors	given	single image	RGB (3)	threshold (maximum)	color histograms	no estimation	ignored	ignored
Machida 2005 [78]	complicated colors	measured	sequence of images	RGB (3)	HDR image	incident positions	estimation of parameters	estimated	constant
Criminisi 2005 [72]	complicated colors	given	sequence of images	RGB (3)	ignored	EPI patterns	no estimation	ignored	ignored
Wang 2006 [79]	complicated colors	measured	sequence of images	RGB (3)	threshold (240)	incident positions	estimation of parameters	ignored	ignored
Present research	complicated colors	given	sequence of images	spectral (81)	replacing saturated value	incident changes	estimation of parameters	ignored	estimated

Chapter 4

Measuring Spectral Images

To acquire the intrinsic reflection properties at the surface of a real object, it is essential for a measurement system to be able to:

i Capture changes in reflection intensity with illumination positions;

ii Capture changes in reflection intensity with surface orientations;

iii Capture the spectral distribution of reflected light at the object surface.

Points [i] and [ii] are based on the theory that reflection intensity varies with illumination and viewing directions, surface roughness, and shape of an object. As we view a glossy object in the real world, the changes in reflection intensity can be observed by arbitrarily moving any one of the three elements (the light source, the camera, and the object surface) while the other two are fixed. To capture reflection properties of an object with complex shapes, it is necessary to tilt the surface orientation of the object so that each of its surfaces can face the camera, while the 3D shape of the object can be obtained by using a rangefinder [15, 79], or structured lighting [29]. Based on the images measured by tilting the surface orientation of objects, the spatial positions, where interreflections occur, may be detected so that interreflections between surfaces of complicated objects can be taken into account while estimating reflectance parameters. For point [iii], either a spectroradiometer or a spectrograph can meet the requirement. However, a line-scanning spectrograph can provide higher resolution, with much less measuring time than a point-based spectroradiometer.

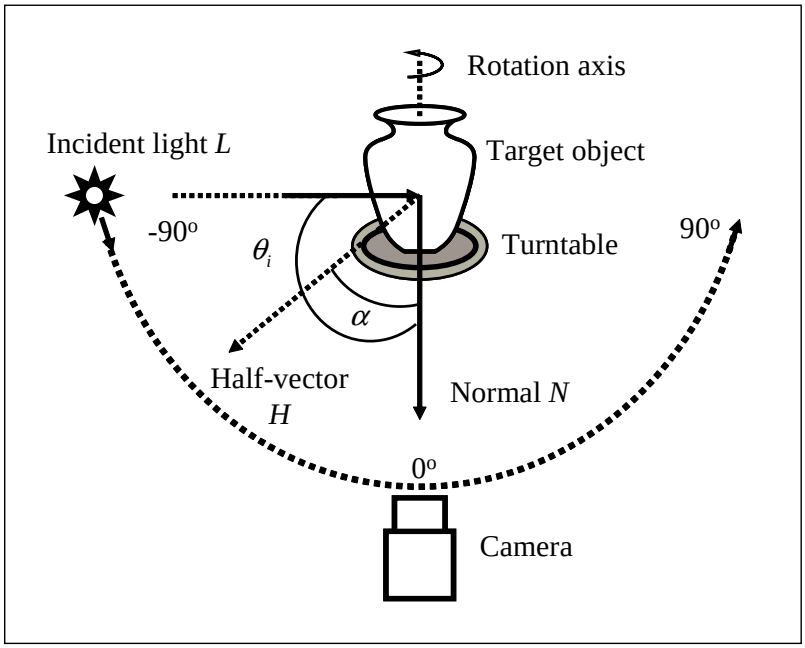

Figure 4.1. Diagram of measurement system

4.1. Measurement System

Since constructing a measurement system to capture reflection properties associated with shapes of a complicated object demands expensive equipment, such as a robotic arm and its controlling system, in this dissertation, a simplified measurement system is constructed using an imaging spectrograph and a moving light source, as shown in Figure 4.1, under the following assumptions:

1. Only one light source is used in a dark space for the experiments;
2. A target object is fixed with one of its surfaces facing the camera, while the light source is moving between -90^o and 90^o;
3. The surface normals of the target object are given, such as by a rangefinder or by structured lighting.

With these assumptions, the ambient lighting and the interreflections between objects and between the surfaces may be embedded into the diffuse and specular reflection occurring at the surface. For simplification, the shape of target objects

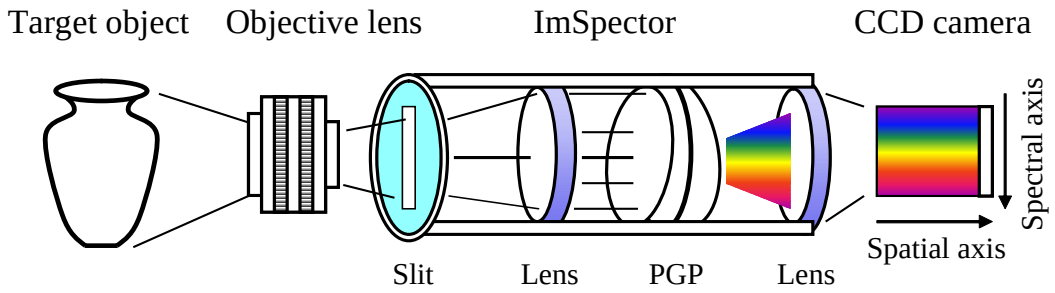

Figure 4.2. Capturing spectral images from imaging spectrograph produced by SPECIM

in this dissertation is approximated to a cylindrical shape with given surface normals. The light source is rotated around the target object, which is placed on a turntable. The imaging spectrograph, equipped with an objective lens and a monochrome CCD camera, is stationary in front of the target object. The rotation axis of the light source overlaps with the center axis of the target object, and the surface normal vector is facing the camera. With these arrangements, the strongest intensity of reflection is observed only when the light source and the camera lie on the same line as the surface normal vector, but in opposite directions.

The reflected light at an object surface enters the slit of the imaging spectrograph through the objective lens, as shown in Figure 4.2, and then disperses via prisms into a spectral distribution in a range of wavelengths. The spectral distribution of the reflected light with the spatial positions for each line of the object surface is captured as an image on the CCD camera. The dynamic range of the imaging spectrograph is dependent on that of the camera, such as 8 bits and 10 bits, and the wavelength range follows the spectral range of the spectrograph, which can be calculated with several optical blocking filters.

Since the imaging spectrograph is a line scanner, which can measure one linear area on the object surface, the target object on the turntable is rotated to acquire spectral images over the whole surface of the object. A TOPCON SR3 spectroradiometer is used for measuring standard spectral distribution of colors at the surface of the target object, to evaluate the spectral distribution estimated

in experiments. TOPCON SR3 is a point-based detector, ranging from 380 nm to 780 nm with 1 nm or 5 nm resolution.

4.2. Preprocessing Spectral Images

With spectral images acquired at each surface line of a target object, several preprocessing steps are necessary to obtain reflection values at each wavelength, with respect to S/N ratio and influence of the instruments used for the measurement system, such as the light source, lens, and camera.

As shown in Equation 1.1, the intrinsic reflection values at each wavelength can be obtained by removing spectral power distribution of illumination and camera properties (including lens sensitivity and prism transmissivity) at each wavelength. A spectral image of a white reference such as a teflon board with given reflectance, captured with the same measurement system in the same illumination, meets the requirement to calibrate the spectral images of target objects, after eliminating CCD dark current from all the spectral images and the whiteboard image. CCD dark current can be obtained in a dark image, measured with no light entering the imaging spectrograph or the CCD camera.

Sequences of calibrated spectral images of a surface line measured at different incident positions are transformed into spectral images with two axes of wavelengths and incident positions, at different spatial positions of the measured surface line, as shown in Figure 4.3.

The linear relationship between wavelength and pixel position at the spectral axis is determined by regression analysis with correlation coefficient $C = 0.999$, using four order interference filters of 449.1 nm, 500 nm, 601.2 nm and 702 nm. The spectral axis is calibrated between 380 nm and 780 nm with respect to the pixel positions.

To maximize the S/N ratio on the spectral images, the spectral image at a single pixel may be smoothed using a moving average method, and reflection values in the spectral image may be averaged across several wavelengths with respect to the spectral axis, without aggravating the spectral resolution. Reflection values at each wavelength are then extracted from the spectral image for each spatial position, as shown in Figure 4.4.

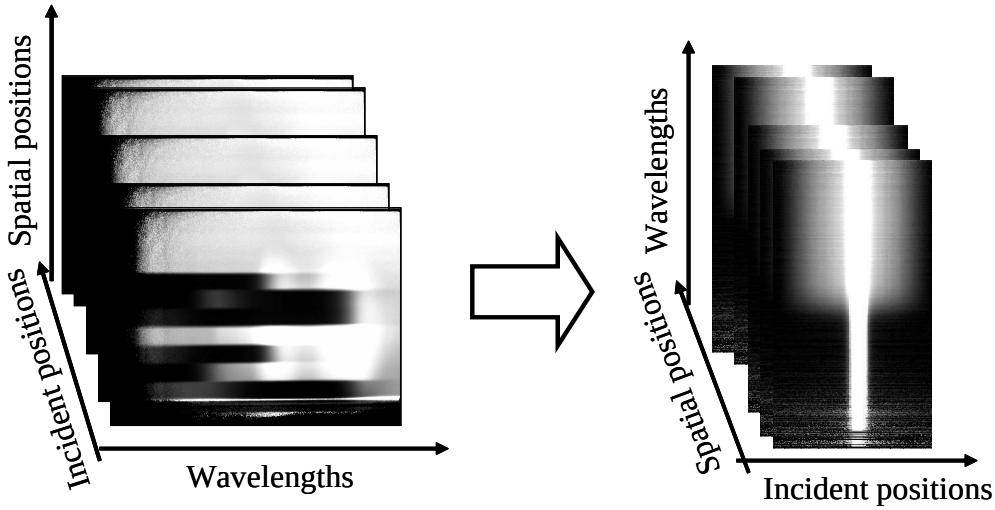

Figure 4.3. Transforming a sequence of calibrated spectral images at different incident positions into spectral images at different spatial positions. Left: The calibrated spectral images at different incident positions; Right: The spectral images at different spatial positions of a surface line

The reflection value at each incident position consists of diffuse and specular reflection components. For dielectric objects, the specular reflection component may be zero at an incident position where only diffuse reflection occurs; however, the diffuse reflection component is nonzero at an incident position where specular reflection occurs. The extracted reflection values at each wavelength of a single point for a surface line across different incident positions, as shown in Figure 4.4 (right), are used for the separation process.

4.3. Conclusions

In this chapter, a measurement system is described to capture the spectral distribution of reflected light at the surface of an object, at different incident positions. The measurement system was constructed comprising an imaging spectrograph which is equipped with a monochrome CCD camera, and a light source that is rotated around the object between -90^o and 90^o. With the spectral images measured from the measurement system, after removing the influence of illumination

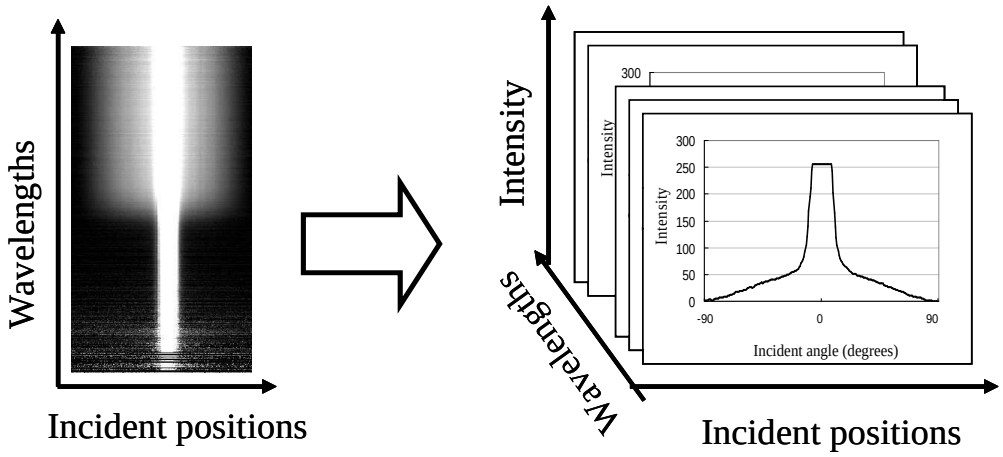

Figure 4.4. Extracting reflectance at each wavelength from a spectral image for each spatial position. Left: A spectral image at a spatial position; Right: Reflection values extracted at each wavelength.

and the CCD camera, reflection values across a sequence of incident positions at each wavelength of a single surface point can be extracted for estimation of reflectance parameters.

Chapter 5

Separating Reflection Values and Estimating Diffuse Reflectance Parameters

Based on the dichromatic reflection model, as shown in Figure 2.8 and Equation 2.9, for dielectric objects, it is assumed that specular reflection is independent of the wavelength of incident radiance. The influences of illumination and the CCD camera used for the measurement are also assumed to be removed by the preprocessing for the spectral images. Therefore, reflection at the surface of an inhomogeneous object can be simplified, as shown in Equation 5.1, when the diffuse and specular reflections are applied to the Lambertian and Torrance-Sparrow reflection models, respectively.

$$E(\lambda, \theta_r) = R_d(\lambda) \cos \theta_i + R_s F(\lambda, \theta_i) G e^{-(\alpha/\sigma)^2} / \cos \theta_r. \tag{5.1}$$

The reflection values $E(\lambda, \theta_r)$ are separated into diffuse and specular reflection components, as shown in Figure 5.1. Then, from the diffuse reflection components, diffuse reflectance parameters $R_d(\lambda)$ are estimated; from the specular reflection components, specular reflectance parameters for intensity R_s and for surface roughness σ are the parameters to estimate. In addition, Fresnel reflectance $F(\lambda, \theta_i)$, including the refractive index $n(\lambda)$ as shown in Equation 2.8, is also estimated from the specular reflection components, according to applications.

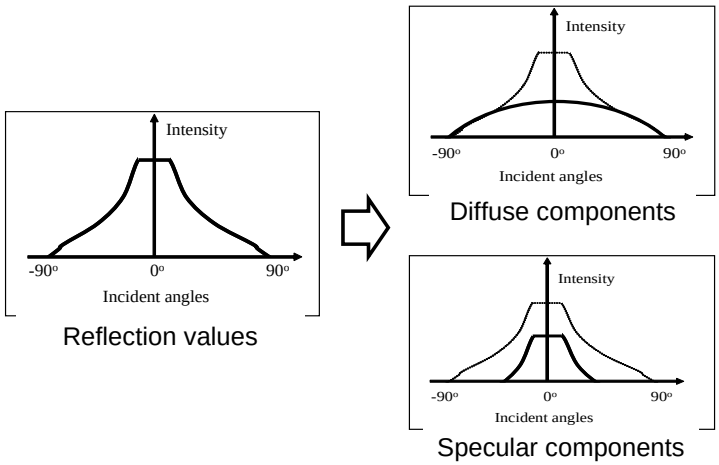

Figure 5.1. Separating reflectance into diffuse and specular reflection components

5.1. Separation Method

A simple method based on the intensity change across the incident positions is described to separate reflection values into diffuse and specular reflection components. Equation 2.6 of the Lambertian reflection model can be transformed logarithmically into a linear form, as shown in Equation 5.2. Reflection values at each wavelength are hypothesized as diffuse only reflection components, and diffuse reflectance parameters are computed by applying the values to the Lambertian reflection model, using the least squares method, as shown in Equation 5.3.

$$log(E_d(\lambda)) = log(R_d(\lambda)) + log(\cos\theta_i). \tag{5.2}$$

$$\varepsilon_d = \sum_{j=0} [log(E'_j(\lambda)) - (log(R_d(\lambda)) + log(\cos\theta_{ij}))]^2, \tag{5.3}$$

where $_j$ represents different incident positions. When the sum of the squares of the difference (SSD) ε_d between the logarithm of the measured reflection values $E'_j(\lambda)$ and the logarithm of the theoretical diffuse reflection components, which are calculated with $R_d(\lambda)\cos\theta_{ij}$, reaches a minimal value, $R_d(\lambda)$ is determined.

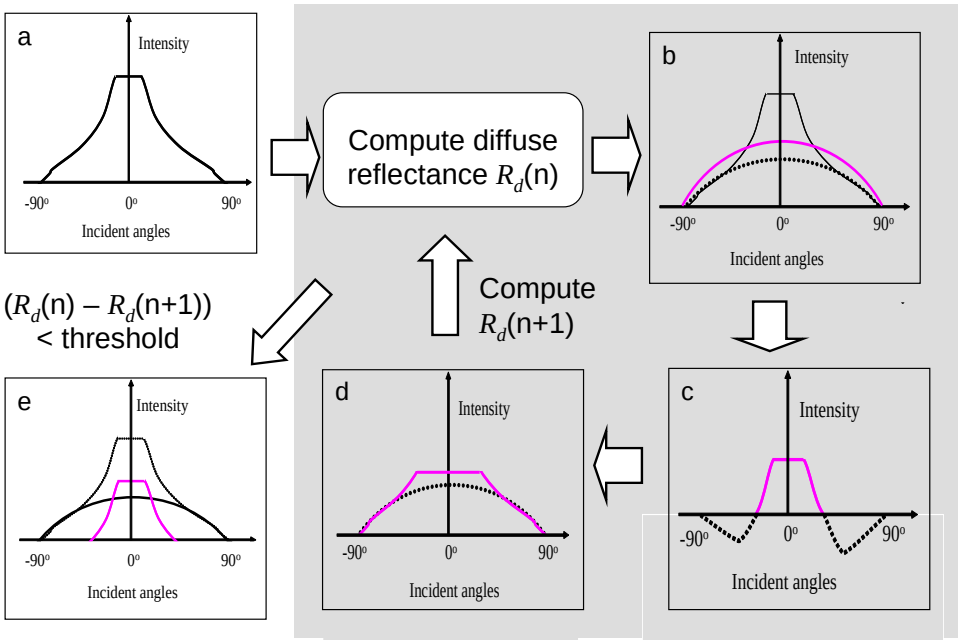

Figure 5.2. Process of separating reflection values into diffuse and specular reflection components

After detecting the maximal value for the reflection values at each wavelength, the separation process is shown as in Figure 5.2.

(1) Subject the reflection values $E'(\lambda)$ lower than a threshold (such as the maximum) to Equation 5.3, and compute a diffuse reflectance parameter, since the reflection values may be saturated;

(2) Synthesize the theoretical diffuse reflection components $E_d(\lambda)$ using this parameter, as shown in Figure 5.2 (b), and subtract $E_d(\lambda)$ from $E'(\lambda)$;

(3) Select values to the right and left sides of the peak position, using values that are larger than a threshold (such as zero) as the specular refection components $E_s(\lambda)$;

(4) Subtract $E_s(\lambda)$ from $E'(\lambda)$, and replace $E'(\lambda)$ with these values, as shown in Figure 5.2 (d);

(5) Repeat from (1) to (4).

When the difference between the current and previous computed diffuse reflectance parameters is lower than a threshold, the reflection values are considered to be separated successfully into the two independent reflection components, as shown in Figure 5.2 (e). With this separation method, the optimal diffuse reflectance parameter is determined as the diffuse reflectance parameter at the current wavelength.

5.2. Experiments with Synthetic Data

To confirm the validity of the separation method and to determine the thresholds used for the separation process, experiments were carried out with synthetic reflection values. The reflection values were synthesized on the basis of the Lambertian reflection model for diffuse reflection components and of the Torrance-Sparrow reflection model for specular reflection components.

In Equation 5.1, $F(\lambda, \theta_i)$ and G were considered as constant values, the values for R_d, R_s, and σ were specified respectively as (100, 155, 10), and the incident angles θ_i were assumed as between -90^o and 90^o with 0.75^o intervals, as shown in Figure 5.3 (Left). Moreover, noise values were generated using random number generation within $\pm 5\%$ of the peak intensity, and added to the reflection values in Figure 5.3 (Left), to yield Figure 5.3 (Right).

Using two types of reflection values, with and without noise, experiments were conducted by subjecting reflection values lower than the maximum for each type to Equation 5.3. The half value of the maximum and the average value for each type of reflection values were also used as the threshold described above in the separation process (1), for comparing computation costs. The diffuse reflectance parameter for each type of reflection values was obtained after two estimations, as shown in Table 5.1 with different thresholds. The experimental results showed that the separation method was efficient for reflection values either with or without noise; and that the threshold for reflection values subjected to the least squares method, their average value showed better advantage than the other two. Therefore, the average value of reflection values can be used for further separation experiments.

Diffuse and specular reflection components were separated as shown in Figure

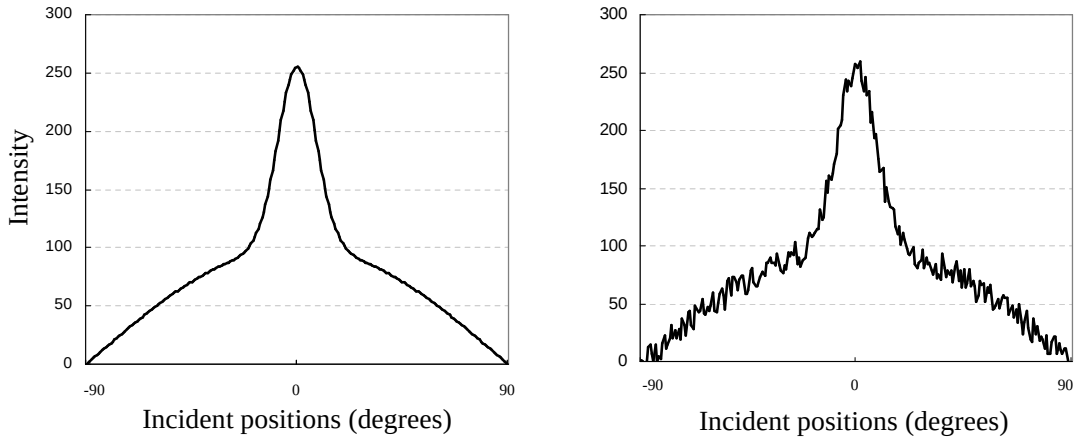

Figure 5.3. Synthetic reflection values. Left: Reflection values without noise; Right: Reflection values with noise.

Table 5.1. Experimental results with synthesized centrosymmetrical reflection values shown in Figure 5.3

	Maximum	Half value	Average value
Without noise	100.00	100.00	100.00
With noise	100.78	100.86	100.54

5.4. In this Figure, specular reflection components are shown in black, diffuse reflection components in magenta, and finally estimated diffuse reflection components in blue. Note that in Figure 5.4 (Left), the estimated and separated diffuse reflection components overlap.

5.3. Experiments with Measured Data

The measurement system was constructed as shown in Figure 5.5. A halogen light source was rotated between -90^o and 90^o at 0.75^o intervals around a target object on a turntable, 1 m away from the rotation axis. The spectral power distribution of the halogen light source is shown in Figure 5.6. The CCD camera equipped with an imaging spectrograph was a [CS3450] monochrome CCD camera, produced by

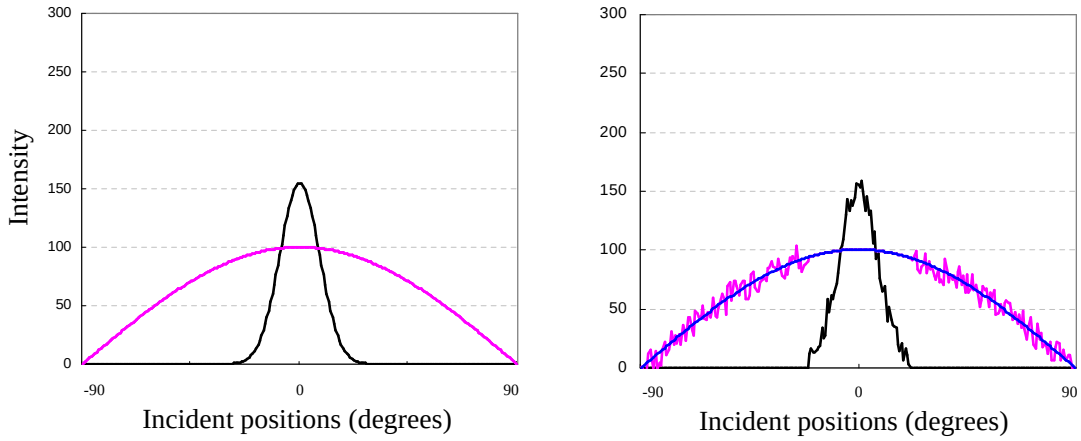

Figure 5.4. Separated diffuse and specular reflection components. Left: Without noise; Right: With noise. For both Left and Right: specular reflection components in black, diffuse reflection components in magenta, and estimated diffuse reflection components in blue

Tokyo Electric Industry, whose spectral response is shown in Figure 5.7.

The target object was placed on another turntable, having the same axis of rotation as the turntable used for the light source, and rotated through 360^o. A color cylinder and a teacup, as shown in Figure 5.8, were measured at 0.625^o and 2.5^o intervals, respectively. The color cylinder was created using matte and glossy types of paper, on each of which there were check patterns of 6 colors (red, green, blue, yellow, magenta, and cyan), as well as several glued areas to vary reflection properties on the surface. The teacup was a cylindrical ceramic structure, with complicated colors and textures on its surface. Since the back of the teacup was entirely white, only spectral images of its front, as shown in Figure 5.8 (Right), were measured.

After removing the influences of illumination and the CCD camera, the spectral images obtained from these two objects were preprocessed as described in Section 4.2. Reflection values at 5-nm intervals between 380 nm and 780 nm were separated into diffuse and specular reflection components, and diffuse reflectance parameters were then estimated at each wavelength. The estimated diffuse reflectance parameters at the surface of matte and glossy paper for blue,

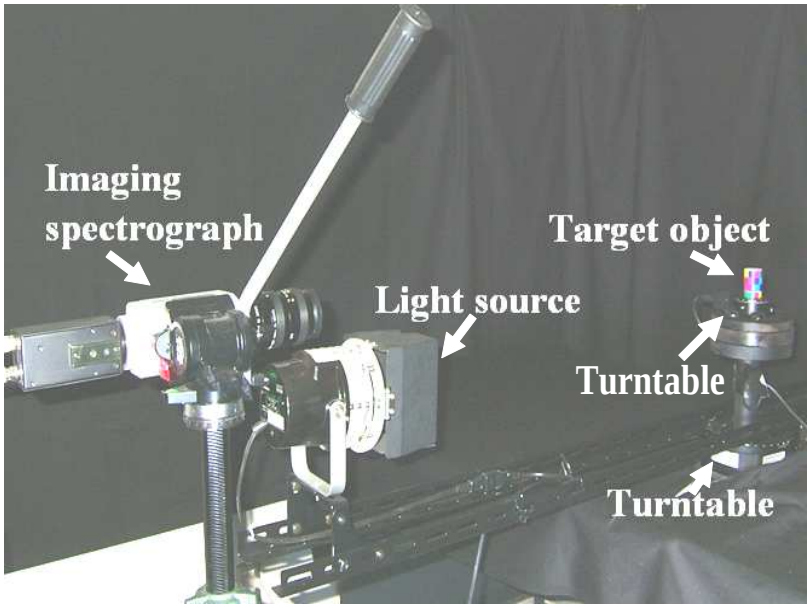

Figure 5.5. Constructed measurement system

cyan, green and magenta, are shown in Figures 5.9 to 5.12, and those at the surface of the glossy paper for yellow and red are shown in Figure 5.13, compared with the standard spectral distribution of the same colors at the surface measured with a spectroradiometer. The diffuse reflectance parameters estimated at 5-nm intervals between 380 nm and 780 nm were computed into R, G, B values using $r(\lambda)$, $g(\lambda)$, and $b(\lambda)$ color matching functions. The opened-up image of the color cylinder and the front image of the teacup are shown in Figure 5.14.

5.4. Discussion

Separating reflection values accurately is crucial for estimation of reflectance parameters. Using a method to separate reflection values and to estimate diffuse reflectance parameters, experiments were carried out with synthetic data and measured data.

From experimental results with synthetic data, as shown in Figure 5.4 and in Table 5.1, reflection values, either with or without noise, can be separated successfully. Diffuse reflectance parameters with the two types of synthetic data are

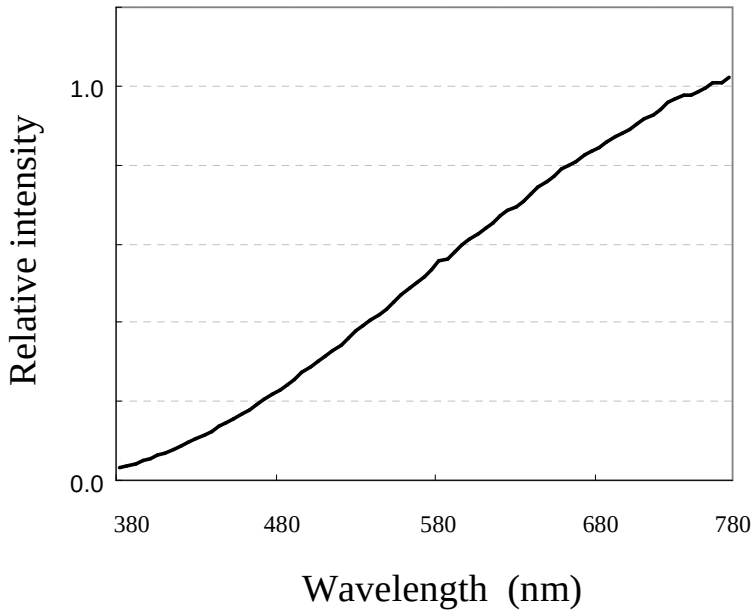

Figure 5.6. Spectral power distribution of the halogen light source

estimated accurately. The average of reflection values can be a reliable threshold in determining reflection values subjected to the least squares method for robust separation and at low computation cost.

From experimental results with measured data, as shown in Figures 5.9 to 5.13, diffuse reflectance parameters estimated for six colors on either matte or glossy paper are in good agreement with the standard spectral distribution of the same colors at those surfaces, in the range of medium and long wavelengths. Diffuse reflectance parameters at short wavelengths are insufficient, since, as shown in Figures 5.6 and 5.7, the halogen light source and the CCD camera used for the experiments are both weak in the range of short wavelengths. This problem can be overcome by using a camera and light source which are strong at short wavelengths, and reducing noise during the measurement of spectral images.

In Figure 5.14, colors on the matte or glossy paper of the cylinder are reproduced sufficiently based on the estimated diffuse reflectance parameters. Colors on the teacup are reproduced adequately. The images in Figure 5.14 look blurred because, since the imaging spectrograph can measure only one line on the surface

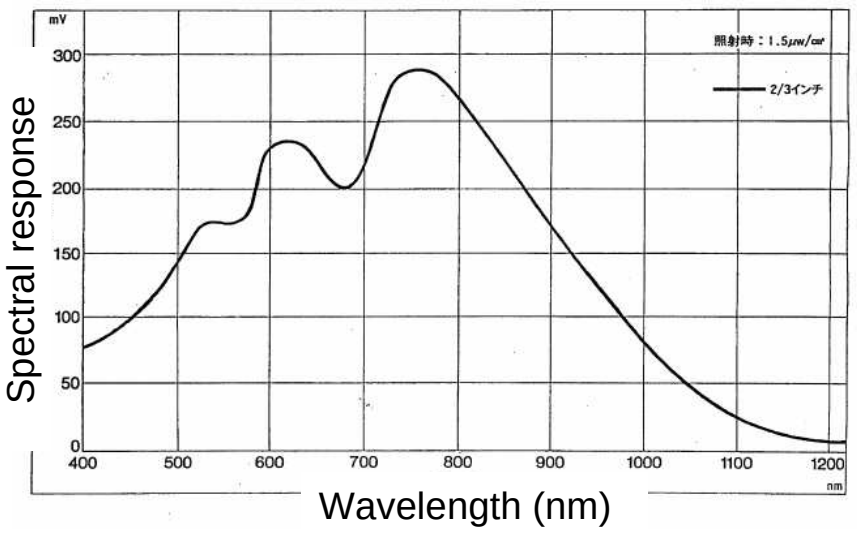

Figure 5.7. Spectral response of the monochrome CCD camera (CS3450)

at a time, the target object was rotated on a turntable at an interval (0.625^o for the teacup, 2.5^o for the color cylinder) rather than continuously. This problem can be improved by mounting an optical lens with high precision on the imaging spectrograph; however, it is difficult to solve this kind of problem using a point-based or line-based light detector.

5.5. Conclusions

In this chapter, a method was described to separate reflection values into diffuse and specular reflection components over a sequence of incident positions, on the basis that, at each surface point, the intensity of specular reflection is dependent on illumination and viewing directions; in contrast, diffuse reflection is independent of viewing direction. By hypothesizing that reflection values are diffuse only reflection components, a least squares method was applied, for reflection values that are lower than the average value, to a logarithmically transformed equation of the Lambertian reflection model. Using this separation method, reflection values can be separated successfully without selecting pixels at which only diffuse reflection occurs, and diffuse reflectance parameters can be estimated at each wavelength automatically when the reflection values are separated. Results from

Color cylinder Teacup

Figure 5.8. Two target objects for experiments

experiments using two types of synthetic data, with and without noise, and using measured spectral images of objects with various colors and gloss, weak or strong, revealed that this method is efficient for separating reflection values and for estimating diffuse reflectance parameters at low computation cost (two or three estimations).

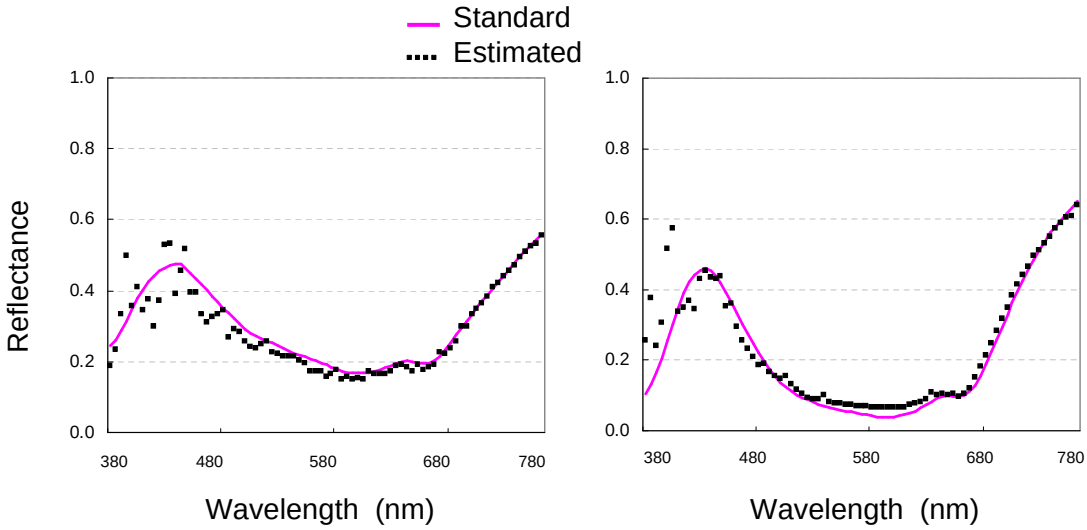

Figure 5.9. Estimated diffuse reflectance parameters on blue paper. Left: Matte paper; Right: Glossy paper

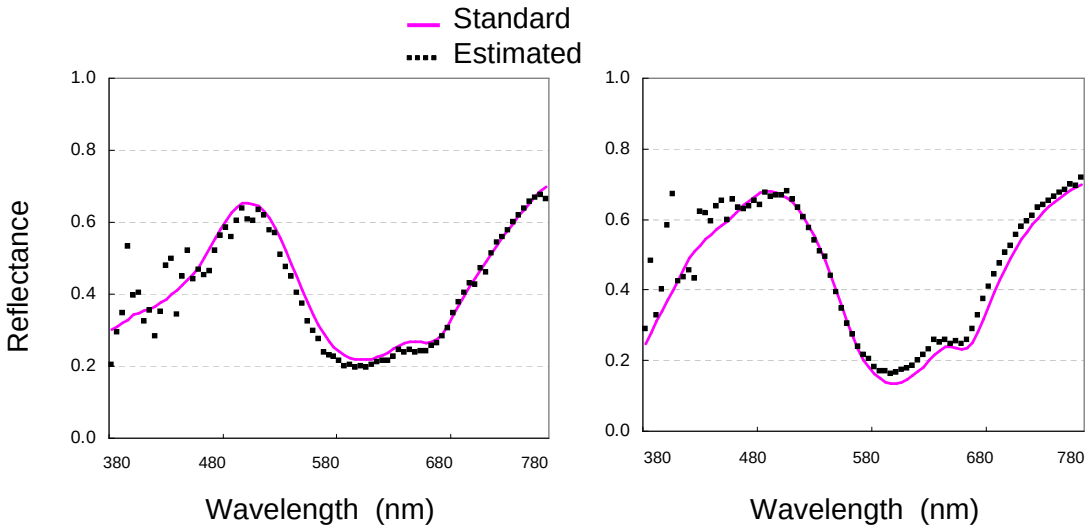

Figure 5.10. Estimated diffuse reflectance parameters on cyan paper. Left: Matte paper; Right: Glossy paper

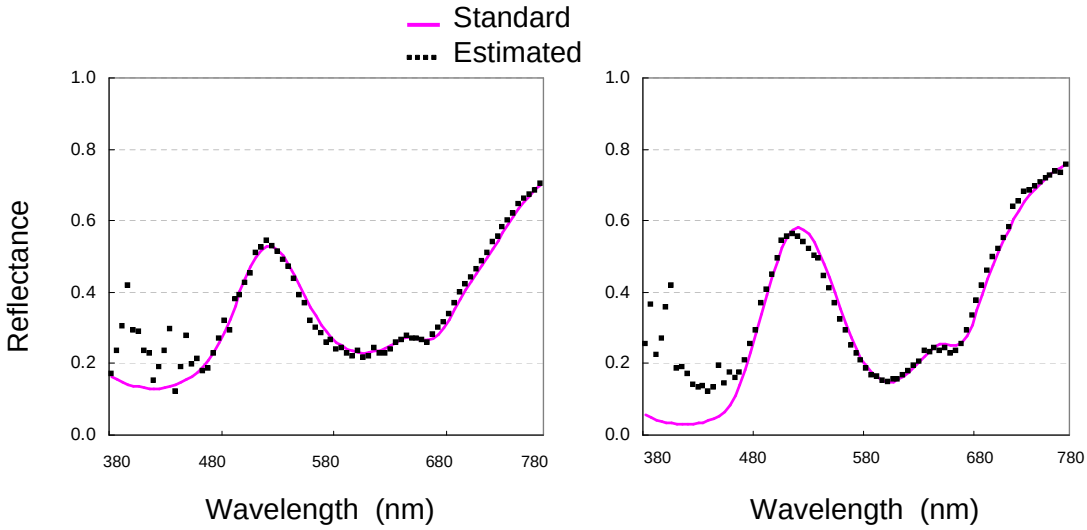

Figure 5.11. Estimated diffuse reflectance parameters on green paper. Left: Matte paper; Right: Glossy paper

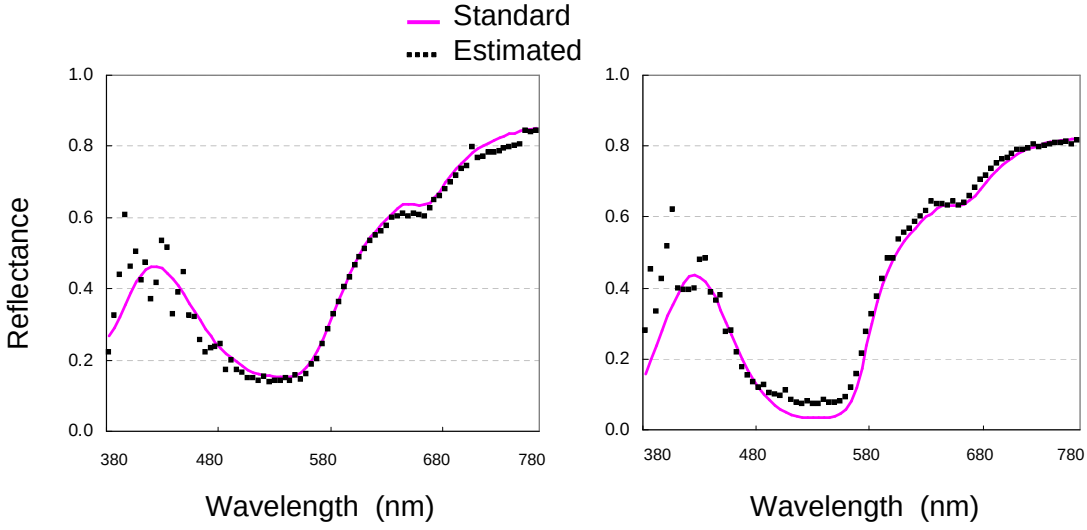

Figure 5.12. Estimated diffuse reflectance parameters on magenta paper. Left: Matte paper; Right: Glossy paper

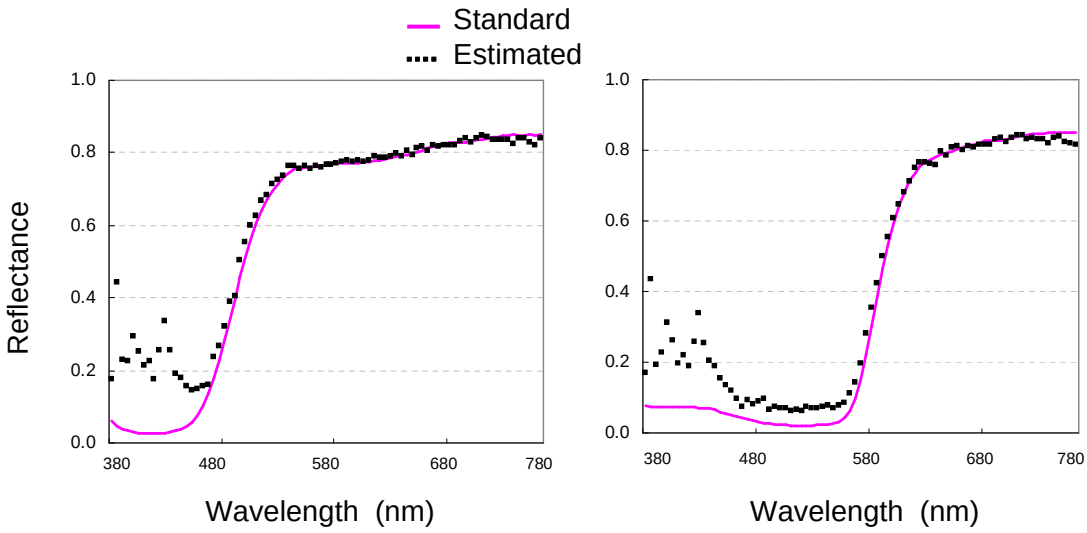

Figure 5.13. Estimated diffuse reflectance parameters on glossy paper. Left: Yellow paper; Right: Red paper

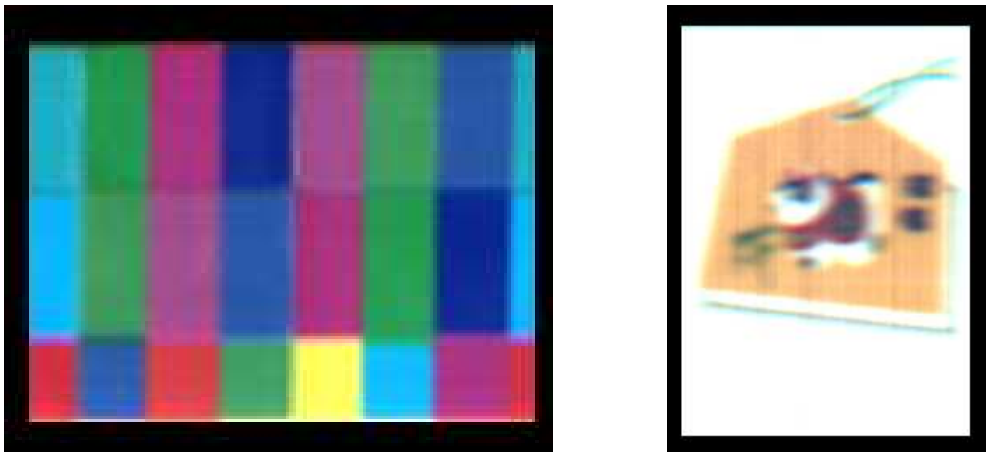

Figure 5.14. RGB values of color cylinder and teacup calculated from estimated diffuse reflectance parameters. a): Opened-up color cylinder; b): Front of teacup

Chapter 6

Estimating Specular Reflectance Parameters

From the separated specular reflection components, specular reflectance parameters for gloss intensity and for surface roughness can be estimated based on reflection models for specular reflection, such as the Torrance-Sparrow model, using existing techniques.

However, the separated specular reflection components may be saturated due to reflection values being saturated at an incident position where specular reflection is strong, or at the smooth surface of an object; and, since diffuse reflection varies with wavelength even for a dielectric inhomogeneous object, specular reflection components are separated with different levels of intensity at each wavelength, as shown in Figure 6.1. Therefore, specular reflectance parameters may be estimated inaccurately by assuming reflection values are unsaturated. A method is described in Section 6.1 to accurately estimate specular reflectance parameters for gloss intensity and for surface roughness even from saturated spectral images.

The Torrance-Sparrow reflection model assumes that the surface of an object is a collection of microfacets, and Fresnel reflectance describes how light is reflected from each microfacet, and how the light affects the specular reflection at a surface point with incident positions. Usually, the Fresnel reflectance $F(\lambda, \theta_i)$ in Equation 2.7 is assumed as a constant value such as 1.0, or is calculated with a given or estimated refractive index. In Section 6.2, a method is introduced to estimate Fresnel reflectance by estimating refractive index at each wavelength

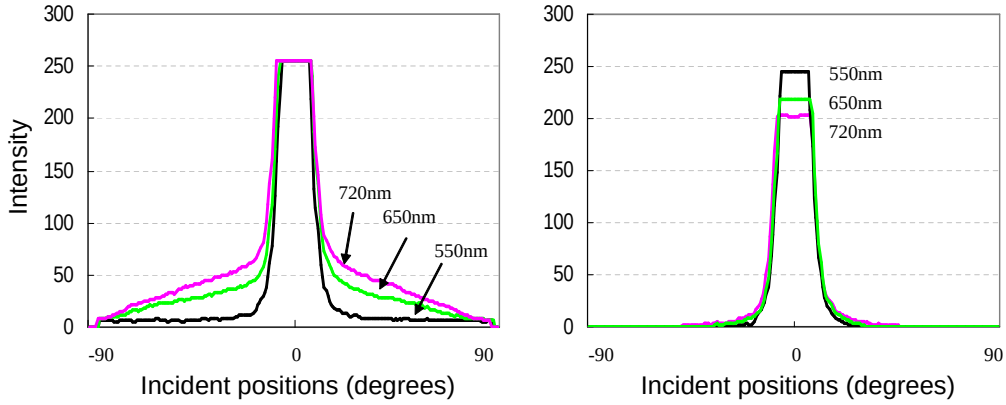

Figure 6.1. Reflection values and the separated specular reflection components at different wavelengths. Left: Reflection values; Right: Separated specular reflection components. For both, at 550 nm in black, 650 nm in green, and 720 nm in magenta

from specular reflection components.

6.1. Estimation of Specular Reflectance Parameters

In Figure 6.1, it is shown that the intensity of the separated specular reflection components may not be the real intensity of specular reflection at the surface point because of the limited dynamic range of a light detector. Since the dichromatic reflection model assumes that specular reflection is independent of wavelength, and since there may be unsaturated reflection values at a particular wavelength at the same surface point, theoretically, we can detect unsaturated reflection values at the particular wavelength and consider specular reflection components separated from them as the specular reflection components of the surface point. However, there are difficulties in determining with a threshold whether reflection values are unsaturated, and in ensuring that unsaturated reflection values at a particular wavelength are usable due to the noise level. Herein a method is described to estimate specular reflectance parameters from specular reflection components,

which are assumed to be separated from saturated reflection values. Naturally, this method is also applicable to specular reflection components separated from unsaturated reflection values.

6.1.1 Proposed Method

The least squares method is applied to estimate specular reflectance parameters from specular reflection components, eliminating values which may be saturated in the original reflection values. The Fresnel reflectance $F(\lambda, \theta_i)$ and the geometrical attenuation G in Equation 2.7 are assumed as constant values, and the equation is transformed logarithmically to a linear form, as shown in Equation 6.1:

$$log(E_s(\lambda, \theta_r)) = log(R_s) - \alpha^2/\sigma^2 - log(\cos\theta_r). \tag{6.1}$$

When SSD ε_s between the logarithm of the separated specular reflection components $E'_{sj}(\lambda, \theta_r)$ and the logarithm of the theoretical specular reflection components, which are calculated with $R_s \exp(-\alpha_j^2/\sigma^2)/\cos\theta_{rj}$, at different incident positions j, reaches a minimal value, specular reflectance parameters R_s and σ are determined, as shown in Equation 6.2:

$$\varepsilon_s = \sum_{j=0} [log(E'_{sj}(\lambda, \theta_r)) - (log(R_s) - \alpha_j^2/\sigma^2 - log(\cos\theta_{rj}))]^2. \tag{6.2}$$

Since specular reflection depends on illumination and viewing directions, it is necessary to adjust the center of saturated values to an incident position of 0^o, where the highest intensity of specular reflection is assumed. The maximal value of specular reflection components at each single wavelength is then detected. Specular reflection components that are smaller than [maximal value − a threshold] are subjected as $E'_{sj}(\lambda, \theta_r)$ in Equation 6.2. Finally, specular reflectance parameters R_s and σ are estimated at each single wavelength. For dielectric objects, R_s and σ can be a representative value, such as a mean value, of the estimated R_s and σ in the range of wavelengths, respectively, at the same surface point.

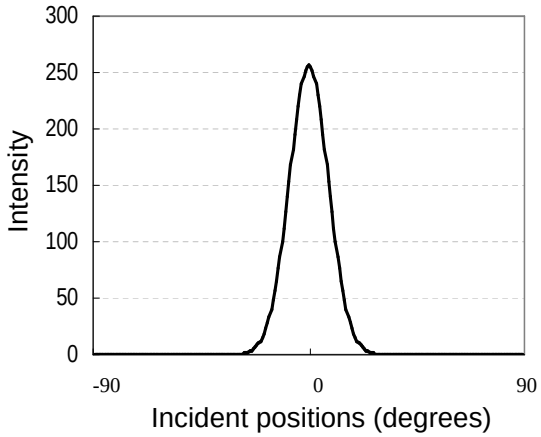

Figure 6.2. Synthetic specular reflection components with $R_s = 255$ and $\sigma = 10$

6.1.2 Experiments with Synthetic Data

To confirm the validity of the method for estimating specular reflectance parameters from specular reflection components, experiments were conducted with synthetic specular reflection components. The specular reflection components were synthesized based on the Torrance-Sparrow reflection model, by supposing that R_s and σ are respectively 255 and 10, and that $F(\lambda, \theta_i)$ and G are 1.0 in Equation 2.7, as shown in Figure 6.2.

The saturation level represents how much the maximal intensity of specular reflection components is saturated with respect to an original intensity. For example, when the maximal intensity of specular reflection components is 25.5, the saturation level is 90% with respect to an expected intensity of 255. Since the intensity of specular reflection components may be truncated at different levels at different wavelengths for the same surface point, specular reflection components with different saturation levels ranging between 0% and 90% of the original intensity of 255 were synthesized, as shown in Figure 6.3 (Left). Furthermore, since measured data usually includes noise, random noise was generated within $\pm 5\%$ of the original intensity of 255, and added to the specular reflection components at each saturation level in Figure 6.3 (Left), as shown in Figure 6.3 (Right).

Subjecting 10 types of specular reflection components without noise to Equation 6.2, specular reflectance parameters R_s and σ were estimated, eliminat-

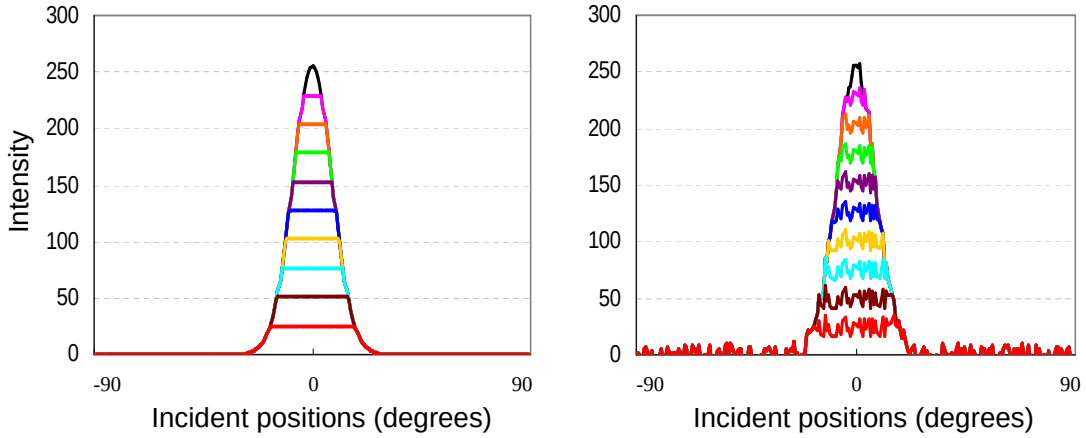

Figure 6.3. Synthetic specular reflection components at different saturation levels. Left: Without noise; Right: With noise. For both, the saturation level ranges [0%, 90%] from top to bottom

ing values which were equal to the maximal value. For 10 types of specular reflection components with noise, the standard deviation (SD) of the random noise was calculated, and specular reflectance parameters R_s and σ were estimated after eliminating values that were larger than [maximal value - SD]. Experimental results using data with and without noise, at 10 saturation levels, are shown in Table 6.1. Note that in Table 6.1, error is calculated as [|original value − estimated|/original value], and represented as %. The original values for R_s and σ are 255 and 10, respectively.

6.1.3 Experiments with Measured Data

The SD of the current dark image was calculated, and the maximal value in separated specular reflection components at each single wavelength was detected. Values that were larger than [maximal value − SD] were considered saturated. Specular reflection components were adjusted so that the center of the saturated values was at the incident position 0^o. Specular reflectance parameters for gloss intensity R_s and for surface roughness σ were estimated at each single wavelength. Since the target objects were dielectric ones, specular reflectance parameters R_s and σ at each surface point were computed as a mean value of R_s and σ esti-

Table 6.1. Estimated R_s and σ using synthetic specular reflection components with and without noise (original values for R_s and σ are 255 and 10).

	Without noise				With noise			
Saturation level	Estimated R_s	Error in R_s (%)	Estimated σ	Error in σ (%)	Estimated R_s	Error in R_s (%)	Estimated σ	Error in σ (%)
0%	255.0	0.0	10.0	0.0	254.05	0.37	10.06	0.6
10%	255.0	0.0	10.0	0.0	254.49	0.20	10.06	0.6
20%	255.0	0.0	10.0	0.0	253.61	0.55	10.05	0.5
30%	255.0	0.0	10.0	0.0	254.58	0.16	10.06	0.6
40%	255.0	0.0	10.0	0.0	254.35	0.25	10.06	0.6
50%	255.0	0.0	10.0	0.0	245.55	3.71	10.10	1.0
60%	255.0	0.0	10.0	0.0	266.29	4.43	10.14	1.4
70%	255.0	0.0	10.0	0.0	268.33	5.23	10.15	1.5
80%	255.0	0.0	10.0	0.0	258.32	1.30	10.10	1.0
90%	255.0	0.0	10.0	0.0	232.95	8.65	9.97	0.3

mated at each single wavelength, respectively. The estimated specular reflectance parameters R_s and σ of the color cylinder are shown in Figure 6.4, and those of the teacup in Figure 6.5. In Figures 6.4 and 6.5, estimated R_s values larger than 410.90 are represented in white. The larger the values of R_s are, the stronger the specular reflection is at the surface point; and the larger the values of σ are, the rougher the surface of the target object is.

Reflection values reproduced using the estimated diffuse reflectance parameter R_d, specular reflectance parameters R_s and σ at 580 nm and 670 nm of different surface points are shown in Figure 6.6, compared with the extracted reflection values from the spectral images at the same surface points. The diffuse reflectance parameter R_d, specular reflectance parameters R_s and σ at 580 nm are estimated as (0.21, 388.98, 4.02), and those at 670 nm as (0.12, 644.62, 15.32).

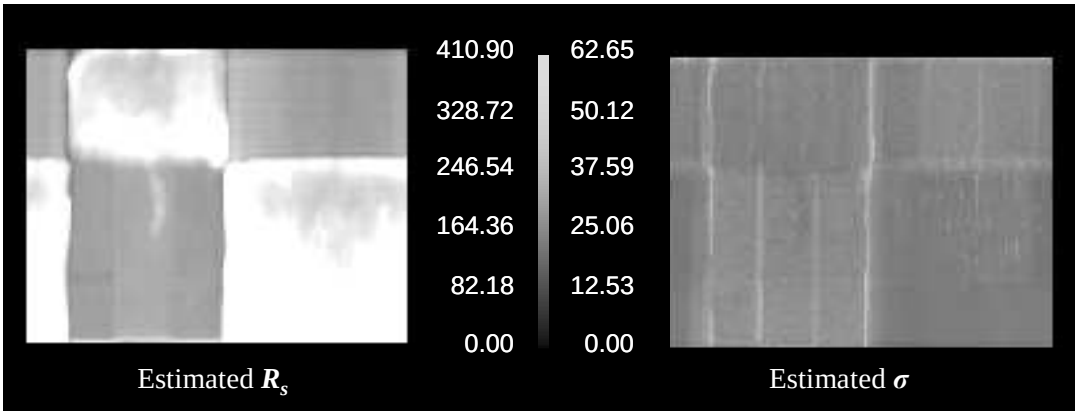

Figure 6.4. Estimated specular reflectance parameters R_s and σ of color cylinder

6.1.4 Discussion

Using the method to estimate specular reflectance parameters from saturated specular reflection components, experiments were carried out using synthetic data at 10 saturation levels, either without or with noise, and using specular reflection components separated from the measured reflection values.

As shown in Table 6.1, experimental results using synthetic data without noise showed that specular reflectance parameters either R_s or σ are estimated to be the same as the original values at any saturation level, with no error. Experimental results using synthetic data with noise showed that specular reflectance parameters R_s and σ were estimated accurately for the data at saturation levels above 40%, with less than 1% error in the original values for R_s and σ; parameters R_s and σ were estimated sufficiently even at other saturation levels, with less than 2% error in the original value for σ and less than 10% error for R_s.

The experimental results using synthetic specular reflection components at different saturation levels verified that this method enables efficient estimation of specular reflectance parameters for gloss intensity and for surface roughness, from either saturated or unsaturated specular reflection components.

Experimental results using the separated specular reflection components, as shown in Figure 6.4, showed that physical characteristics of the surfaces of the color cylinder are reproduced sufficiently. Physical properties of glossy paper, matte paper, the boundaries of the two types of paper, and the glued areas on

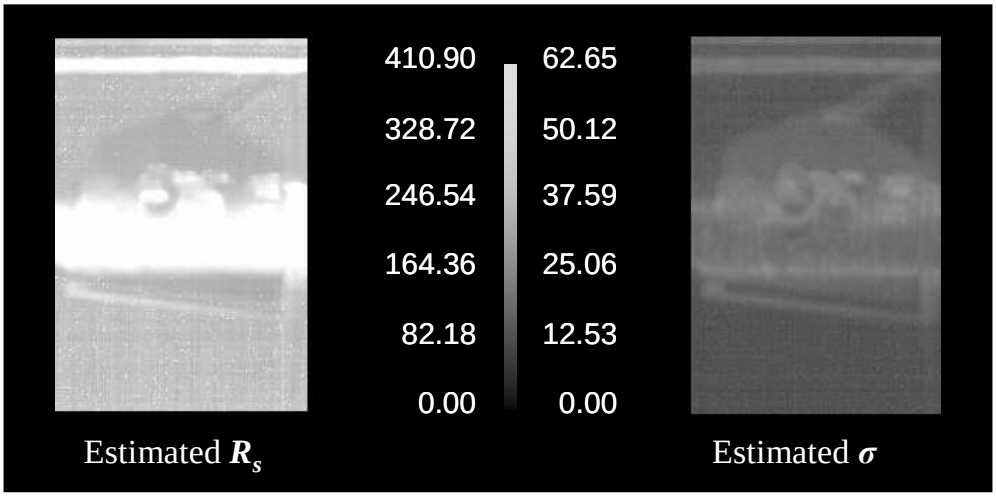

Figure 6.5. Estimated specular reflectance parameters R_s and σ of the teacup

either matte or glossy paper, are estimated adequately. For the teacup shown in Figure 6.5, the specular reflectance parameters for surface roughness σ were estimated accurately; areas where strong specular reflection was measured were appeared bright for the specular reflectance parameters for gloss intensity R_s, and the other areas appeared darker, since the teacup was approximated as an ideal cylinder for the estimation. For measuring strong specular reflection at the other areas, it is necessary to tilt surface orientations of the target object while using the same settings for the light source and imaging spectrograph in the measurement system.

As shown in Figure 6.6, the reflection values reproduced using diffuse reflectance parameters R_d, specular reflectance parameters R_s and σ are in good agreement with the measured reflection values; and, at incident positions close to 0^o, the reproduced reflection values replaced values that were saturated in the measured reflection values because of the limited dynamic range of the CCD camera.

The experimental results with specular reflection components separated from the measured spectral images demonstrated that specular reflectance parameters for gloss intensity and for surface roughness can be estimated adequately when either weak or strong specular reflection is present, and even when the strong specular reflection is saturated in input images.

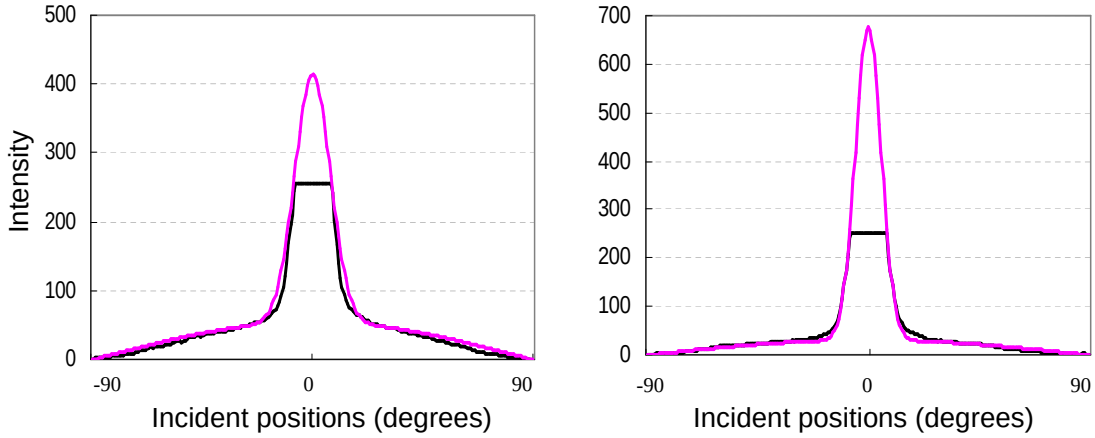

Figure 6.6. Estimated reflection values using the estimated reflectance parameters, compared with those extracted from spectral images at the same wavelengths of surface points. Left: at 580 nm; Right: at 670 nm. For both, estimated and measured reflection values are represented separately in magenta and in black

6.2. Estimation of Fresnel Reflectance

Fresnel reflectance can be computed with given refractive indices for dielectric materials in Equation 2.8. The refractive indices of transparent materials can be measured using a refractometer; however, there are difficulties in measuring the refractive indices of opaque surface materials and in having a reliable list of refractive indices for most materials, since refractive indices are dependent on wavelength, and on conditions such as temperature and purity, at different surface points of an inhomogeneous object.

Using the method described in Section 5.1 to separate reflection values and to estimate diffuse reflectance parameters at each single wavelength of each surface point, the refractive index can be estimated at each wavelength from unsaturated reflection values measured at normal direction in the simplified Equation 3.1. However, it is difficult to capture reflection properties at normal directions of an object, and to assure the reflection values are unsaturated.

A new method is introduced to estimate refractive index, and to estimate specular reflectance parameters R_s and σ at each wavelength from saturated specular

reflection components, given that the method described in Section 6.1 is efficient for estimating specular reflectance parameters from specular reflection components at different saturation levels, while the Fresnel reflectance and geometric attenuation factor are assumed as 1.

6.2.1 Proposed Method

By assuming the geometric attenuation factor as a constant value, the equation of the Torrance-Sparrow reflection model is transformed logarithmically into a linear form, as shown in Equation 6.3, and Equation 6.2 is modified to Equation 6.4 with the same definition:

$$log(E_s(\lambda, \theta_r)) = log(R_s) + log(F(\lambda, \theta_i)) - \alpha^2/\sigma^2 - log(\cos\theta_r), \tag{6.3}$$

$$\varepsilon_s = \sum_{j=0} [log(E'_{sj}(\lambda, \theta_r)) - (log(R_s) + log(F(\lambda, \theta_i)) - \alpha_j^2/\sigma^2 - log(\cos\theta_{rj}))]^2. \tag{6.4}$$

Fresnel reflectance is calculated in terms of Equation 2.8 with given refractive indices ranging between 1.3 and 2.0 for a dielectric object. The flowchart of the process to estimate refractive index n, specular reflectance parameters R_s and σ is shown in Figure 6.7.

First, Fresnel reflectance is computed with an initial n_0, and specular reflectance parameters R_s and σ are estimated with the method described in Section 6.1. SSD ε_s is then computed between measured specular reflection components and theoretical specular reflection components, which are calculated using the computed Fresnel reflectance and the estimated R_s and σ in Equation 2.7. The process is repeated by replacing n at 0.001 intervals between 1.3 and 2.0, and a minimal SSD is then detected. At the same time, a refractive index n and specular reflectance parameters R_s and σ are determined.

6.2.2 Experiments with Synthetic Data

To confirm the validity of the proposed method, experiments were conducted using synthetic specular reflection components. The specular reflection components

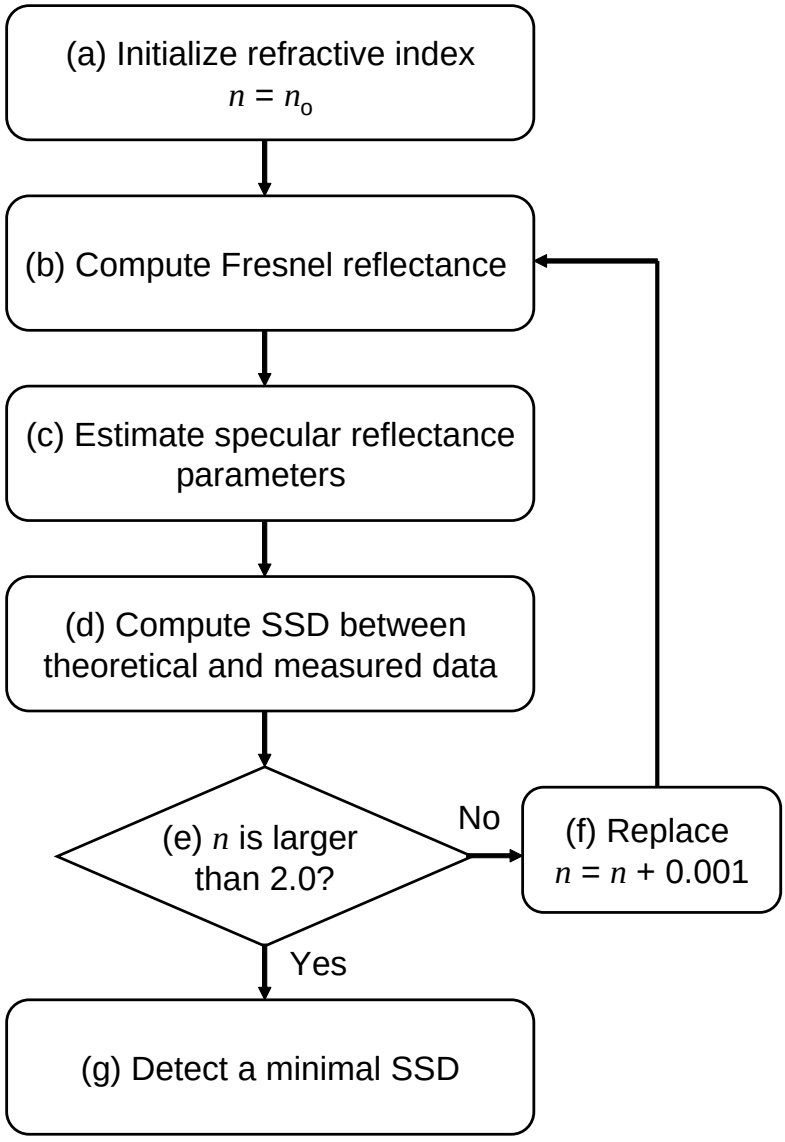

Figure 6.7. Flowchart for estimating refractive index and specular reflectance parameters

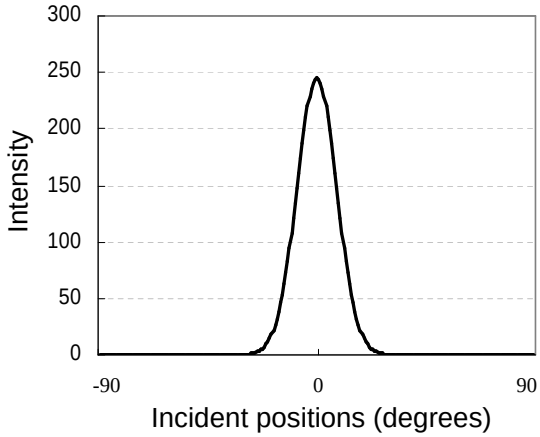

Figure 6.8. Synthetic specular reflection components with $n = 1.5$, $R_s = 255$, and $\sigma = 10$

were synthesized based on the Torrance-Sparrow reflection model in Equations 2.7 and 2.8, with R_s, σ, and n as (255, 10, 1.5), as shown in Figure 6.8. In a similar way to that described in Section 6.1, specular reflection components were synthesized with 10 saturation levels of [0%, 90%], without noise and with noise randomly generated within ±5% of the original intensity of 255. The saturated specular reflection components are shown in Figure 6.9. Data without noise is at Left and that with noise at Right; for data with or without noise, saturation levels range between 0% and 90% from top to bottom.

Using 10 types of saturated specular reflection components either without or with noise, specular reflectance parameters R_s and σ were estimated, while assuming $F(\lambda, \theta_i)$ and G as 1. The estimation results are shown in Table 6.2.

Using 10 types of saturated specular reflection components either without or with noise, refractive index n, specular reflectance parameters R_s and σ were estimated using the method proposed in this section. The estimation results are shown in Table 6.3.

6.2.3 Discussion

Using the method to estimate refractive index and specular reflectance parameters at each wavelength, experiments were carried out using synthetic specular

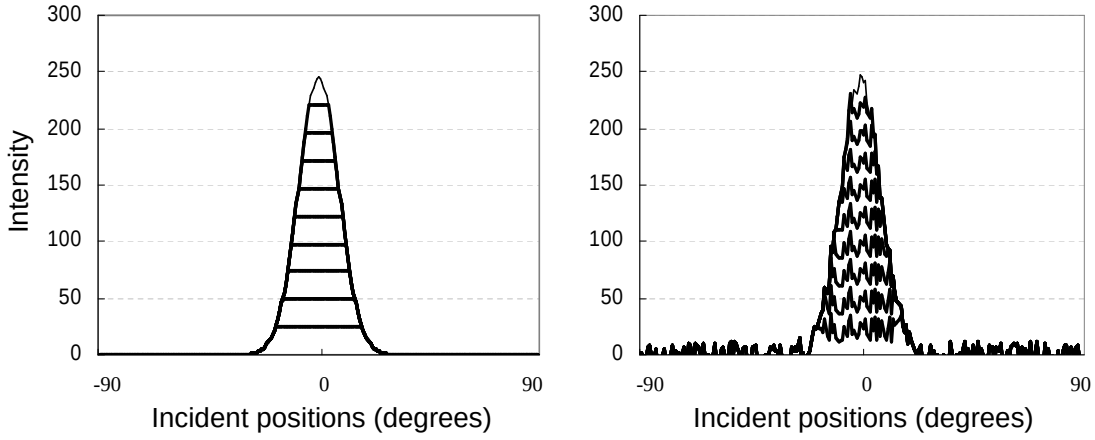

Figure 6.9. Synthetic specular reflection components at different saturation levels. Left: Without noise; Right: With noise. For both, the saturation level ranges [0%, 90%] from top to bottom

reflection components at 10 saturation levels either without or with noise.

From specular reflection components without noise, specular reflectance parameters R_s and σ as shown in Tables 6.2 and 6.3, and refractive index n as shown in Table 6.3, were estimated accurately at any saturation level.

From specular reflection components with noise, at saturation levels above 80%, the specular reflectance parameters R_s and σ in Table 6.2 were estimated sufficiently with around 10% and 1.5% errors with respect to the original values for R_s and σ, respectively. In Table 6.3, the specular reflectance parameters for gloss intensity R_s were estimated with less error in the original value for R_s, and the specular reflectance parameters for surface roughness σ were estimated with comparable sufficiency as in Table 6.2; however, the refractive indices n were estimated inaccurately.

Experimental results demonstrated that specular reflectance parameters for surface roughness can be estimated stably; and those for gloss intensity can be refined by taking Fresnel reflectance into account for given refractive indices of surface materials. The new method can be effective for estimating specular reflectance parameters for gloss intensity using the stability of estimating parameters for surface roughness. On the other hand, more work is required to estimate

Table 6.2. Estimated R_s and σ using synthetic specular reflection components with and without noise (original values for R_s, σ, and n are 255, 10, and 1.5)

	Without noise				With noise			
Saturation level	Estimated R_s	Error in R_s (%)	Estimated σ	Error in σ (%)	Estimated R_s	Error in R_s (%)	Estimated σ	Error in σ (%)
0%	244.8	4.0	10.0	0.0	239.67	6.0	9.95	0.5
10%	244.8	4.0	10.0	0.0	238.92	6.3	9.94	0.6
20%	244.8	4.0	10.0	0.0	237.04	7.0	9.93	0.7
30%	244.8	4.0	10.0	0.0	234.67	7.9	9.91	0.9
40%	244.8	4.0	10.0	0.0	235.58	7.6	9.91	0.9
50%	244.8	4.0	10.0	0.0	227.19	10.9	9.85	1.5
60%	244.8	4.0	10.0	0.0	245.86	3.6	10.00	0.0
70%	244.8	4.0	10.0	0.0	247.15	3.1	10.00	0.0
80%	244.8	4.0	10.0	0.0	242.20	5.0	9.98	0.2
90%	244.8	4.0	10.0	0.0	144.36	43.4	9.22	7.8

refractive index at each wavelength, based on the complicated Equation 2.8.

6.3. Reproducing Reflection Properties

Using diffuse reflectance parameters estimated at each 5-nm interval in Section 5.3, diffuse reflection in RGB values of the cylinder and teacup were reproduced based on the Lambertian reflection model, as shown in Figure 6.10. Using specular reflectance parameters for gloss intensity and for surface roughness estimated in Section 6.1, specular reflection in RGB values of the two objects was reproduced based on the Torrance-Sparrow reflection model, assuming Fresnel reflectance and the geometric attenuation factor as 1. Based on the dichromatic reflection model, reflection properties (color and gloss) of the color cylinder and of the teacup are shown in Figure 6.11.

In Figures 6.10 and 6.11, colors of the glossy and matte paper of the cylinder are reproduced sufficiently, and gloss on matte and glossy paper is reproduced

Table 6.3. Estimated n, R_s and σ using synthetic specular reflection components with and without noise (original values for n, R_s, and σ are 1.5, 255, and 10)

	Without noise			With noise				
Saturation level	Estimated R_s	Estimated σ	Estimated n	Estimated R_s	Error in R_s (%)	Estimated σ	Error in σ (%)	Estimated n
0%	255.0	10.0	1.5	243.81	4.4	9.95	0.5	1.30
10%	255.0	10.0	1.5	243.05	4.7	9.94	0.6	1.30
20%	255.0	10.0	1.5	264.96	3.9	9.92	0.8	1.96
30%	255.0	10.0	1.5	262.48	2.9	9.90	1.0	1.97
40%	255.0	10.0	1.5	263.41	3.3	9.91	0.9	1.96
50%	255.0	10.0	1.5	254.06	0.4	9.85	1.5	1.97
60%	255.0	10.0	1.5	274.71	7.7	9.99	0.1	1.96
70%	255.0	10.0	1.5	275.89	8.2	10.00	0.0	1.96
80%	255.0	10.0	1.5	270.12	5.9	9.98	0.2	1.95
90%	255.0	10.0	1.5	161.00	36.9	9.22	7.8	1.95

as realistically as it appears on a real object: much stronger gloss is observed on glossy than on matte paper in the same illumination and viewing directions, and at the same height of the cylinder. Colors and gloss of the teacup are reproduced adequately; however, the reproduced image is blurred because the imaging spectrograph for measuring spectral images is a line scanner.

Colors and gloss at the back side of the cylinder show dramatic variations in different light sources, as shown in Figure 6.12. In this manner, reflection properties of an object can be reproduced associated with illuminations in a virtual environment where the object is exhibited, while at its side, representing intrinsic reflection properties of the object according to applications.

6.4. Conclusions

In this chapter, two methods, with and without estimation of Fresnel reflectance, are described to estimate specular reflectance parameters for gloss intensity and

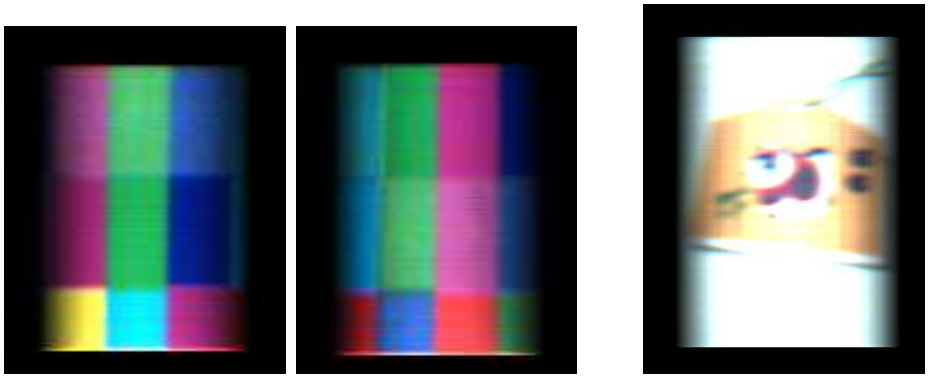

a) Color cylinder b) Teacup

Figure 6.10. Reproduced diffuse reflection of the color cylinder and the teacup

for surface roughness from either unsaturated or saturated specular reflection components. Using the method that assumes Fresnel reflectance as a constant value, experimental results for synthetic specular reflection components, with and without noise, at different saturation levels, and using measured specular reflection components of real objects with weak or strong gloss, have shown that specular reflectance parameters for surface roughness can be estimated accurately, and those for gloss intensity adequately.

Using the method that estimates Fresnel reflectance in terms of the complicated Fresnel equation, experimental results for synthetic specular reflection components, with and without noise, at different saturation levels, have demonstrated that specular reflectance parameters for surface roughness can be estimated accurately; specular reflectance parameters for gloss intensity can be estimated more precisely by taking Fresnel reflectance into account than by assuming Fresnel reflectance as a constant value. However, the refractive index cannot be determined properly with this method because the equation is unsolvable.

Using either of these two methods, intensity of specular reflection components can be estimated by replacing saturated values at positions where highlights are measured because of the limited dynamic range of a CCD camera. Experimental results based on the estimated diffuse and specular reflectance parameters of different objects have revealed that colors and gloss can be reproduced sufficiently.

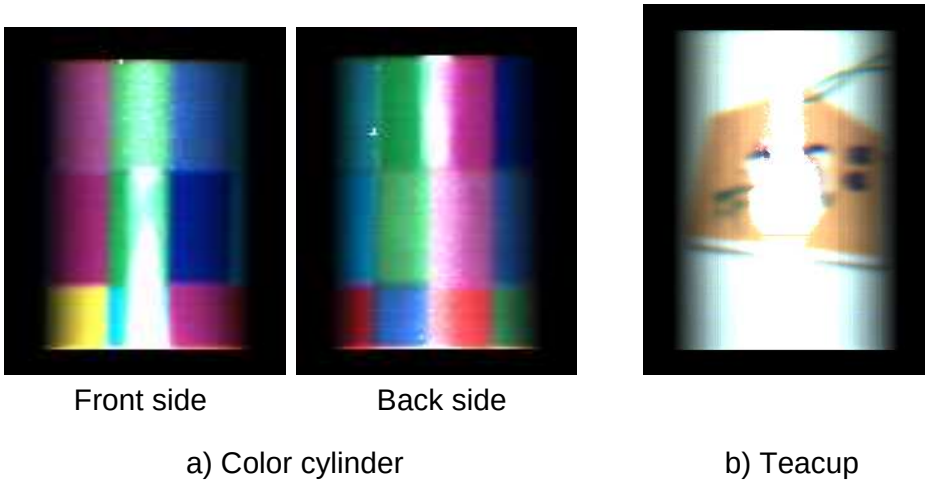

Figure 6.11. Reproduced diffuse and specular reflection of the color cylinder and the teacup

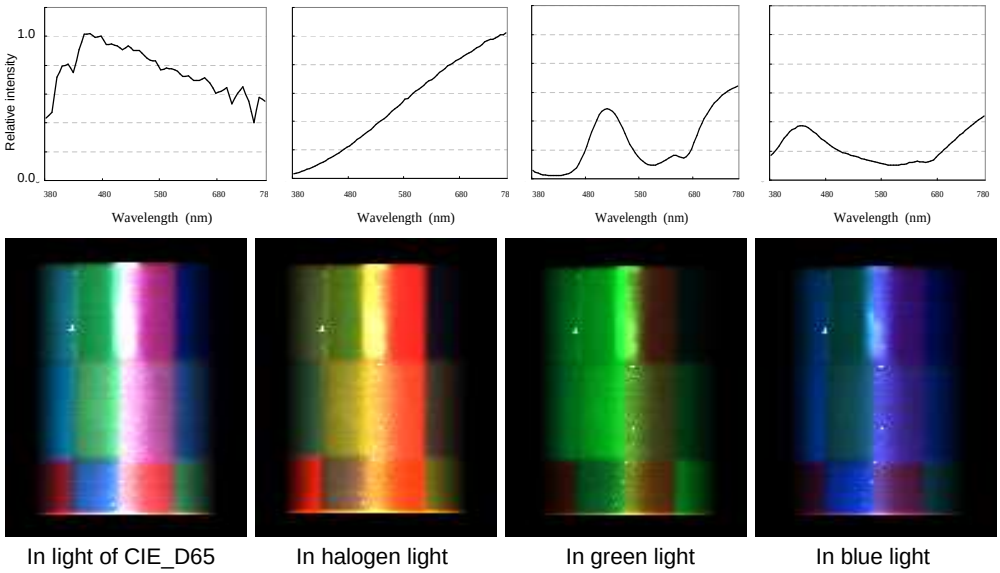

Figure 6.12. Various appearances of reflection properties at the back side of color cylinder in different light sources

Chapter 7

Discussion

The objectives of the present study were to acquire physically sufficient information about colors and gloss at the surface of an object; to estimate accurate reflectance parameters; and to reproduce reflection properties using accurately estimated reflectance parameters, associated with illuminations in a virtual environment such as a digital museum for cultural heritage artifacts.

The experimental results revealed that, by applying the measurement system and the methods described in this dissertation, diffuse reflectance parameters for color can be estimated accurately at each wavelength using spectral images, without the influence of illumination and the CCD camera used for the measurement; specular reflectance parameters for gloss intensity and for surface roughness can be estimated sufficiently from either saturated or unsaturated specular reflection components, replacing values that are saturated due to the limited dynamic range of a light detector.

Discussion now is focused on several assumptions in the present work, and on possible solutions to these assumptions.

Given geometrical information Geometrical shape is a fundamental attribute of an object, and greatly affects reflection properties, especially gloss, including interreflections. In the measurement system, it is assumed that each surface of an object with a complicated shape is measured either by tilting its surface orientation toward the imaging spectrograph, which is fixed in front of the object; or by moving the imaging spectrograph in arbitrary directions around the object with

an instrument such as a robotic arm, when the object is fixed. The geometrical shape of objects may be given, such as for commercial goods in online shops; however, information about the shape of cultural heritage artifacts is often unknown. It is necessary to measure reflection properties associated with the shape of an object, using a rangefinder or using structured light. Moreover, on the basis of information about shape, interreflections may be taken into account in separating diffuse and specular reflection components, by selecting surface points where diffuse or specular interreflections occur, according to incident positions.

Parallel incident light Specular reflection varies sensitively with illumination and viewing directions; therefore, it is important to measure reflection properties precisely by moving the light source/camera in directions on a hemisphere, or by tilting surface orientations of the object in arbitrary directions, without assumptions such as that incident light arriving at each surface point of an object is parallel, as in existing literature in CG&CV.

The dichromatic reflection model In the real world, objects are created not only with opaque dielectric materials, but also with various materials such as transparent materials or metals. Since diffuse reflectance parameters for colors, and specular reflectance parameters for gloss intensity and for surface roughness, can be estimated at each wavelength, the estimation methods described in this dissertation can be extended for various materials. However, the separation method requires an appropriate model, which can interpret reflection and other interactions between incident light and surface materials, such as absorption for metals and refraction for transparent materials, instead of the dichromatic reflection model.

Constant $F(n(\lambda), \theta_i)$ and G in the Torrance-Sparrow reflection model Fresnel reflectance and the geometrical attenuation factor in the Torrance-Sparrow reflection model may have a large influence on the intensity of specular reflection at very rough surfaces of objects such as cloth and clay. Fresnel reflectance can be computed with a given refractive index at each wavelength. However, it is difficult to estimate refractive indices from specular reflection components which are saturated, using the unsolvable Fresnel equation. New methods are desirable for obtaining the refractive index at each wavelength of a single surface point.

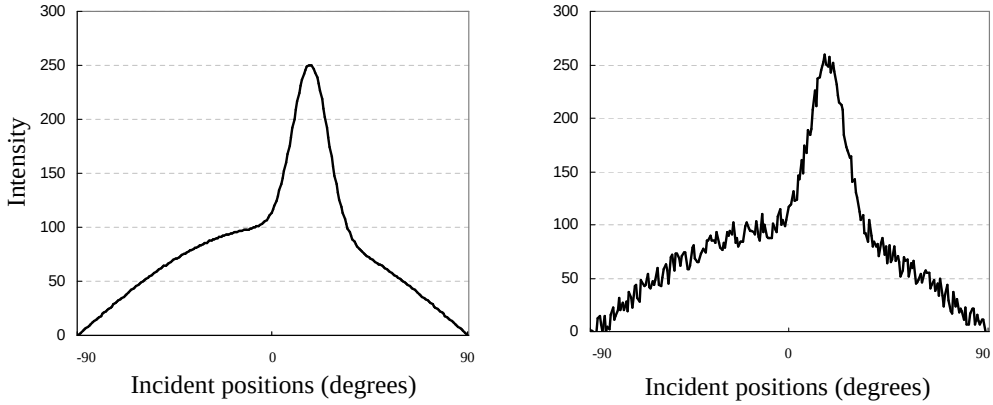

Figure 7.1. Asymmetrical reflection values. Left: Reflection values without noise; Right: Reflection values with noise

The geometrical attenuation factor may be estimated by modeling interreflections between microfacets at the rough surface of an object, when reflection properties can be measured in arbitrary illumination and viewing directions.

Symmetrical reflection values The measurement system described in the present work has assumed that the peak intensity of reflected light is measured at 0^o with a light source moving between -90^o and 90^o. Using the measured spectral images or symmetrically synthetic reflection values, the separation method in Section 5.1 has shown its efficiency. To confirm that the method can be applied for asymmetrical reflection values, which are often obtained when surface normals of an object with complicated shapes are not on the same line as the optical axis of the camera, with and without noise, two types of asymmetrical reflection values were synthesized based on the reflection models, with R_d, R_s, and σ as (100, 155, 10) in Equation 5.1, in a similar way to that used for synthesizing the symmetrical data described in Section 5.2. The results are shown in Figure 7.1.

Experiments using these two types of reflection values were conducted by subjecting reflection values lower than the maximum, or the half value of the maximum, or the average value of each type of reflection values, to Equation 5.3. Diffuse reflectance parameters with each of the thresholds were estimated, as shown in Table 7.1; diffuse and specular reflection components were separated, as shown in Figure 7.2.

Table 7.1. Experimental results with synthesized asymmetrical reflection values shown in Figure 7.1

	Maximum	Half value	Average value
Without noise	100.00	100.00	100.00
With noise	101.28	101.11	100.54

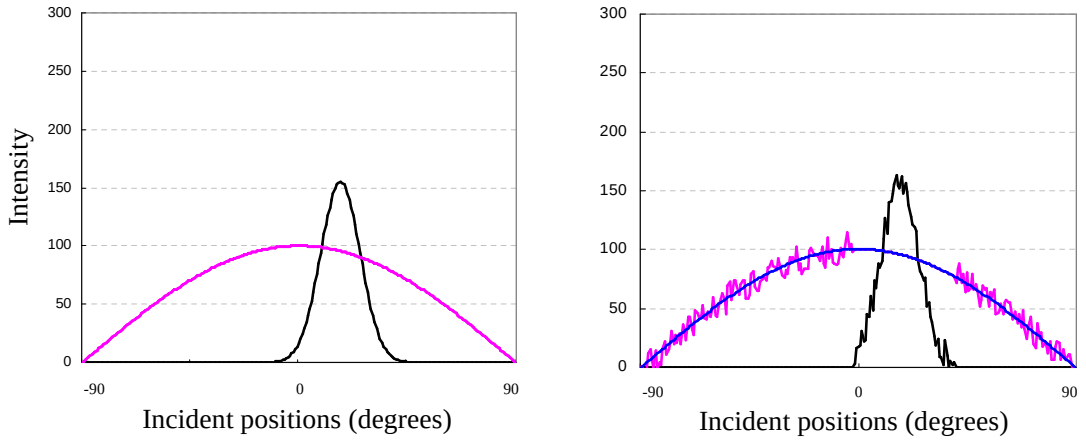

Figure 7.2. Separated diffuse and specular reflection components from asymmetrical reflection values. Left: Without noise; Right: With noise. For both Left and Right: specular reflection components in black, diffuse reflection components in magenta, and estimated diffuse reflection components in blue

The experimental results in Table 7.1 and Figure 7.2 show that, by applying the separation method, asymmetrical reflection values can also be separated successfully; diffuse reflectance parameters can be estimated accurately at low computation cost. However, since specular reflection is dependent on the incident and viewing directions, it is necessary to adjust the peak position, or center position for saturated values, of specular reflection components to 0^o for estimating specular reflectance parameters accurately.

As described above, accurate reflection properties at surfaces of an object can be captured without assumptions, in arbitrary illumination and viewing directions on a hemisphere, associated with measuring the shape of the object. However,

measuring reflection properties perfectly for numerous combinations of illumination and viewing directions requires a large amount of measurement time and high storage capacity for vast numbers of input images. This problem is commonly encountered in this kind of work in CG&CV, although it can be addressed by accurately estimating various kinds of parameters, such as for diffuse and specular reflection, from numerous amount of input images using the separation and estimation methods described in the present work.

Chapter 8

Conclusions

8.1. Summary

To capture reflection properties accurately at the surface of an object, and to estimate reflectance parameters precisely, a measurement system with an imaging spectrograph fixed in front of the target object, and a light source rotating around the target object between -90^o and 90^o, has been constructed to measure spectral images at each incident position.

A separation method has been introduced to separate reflection values after removing the influence of illumination and camera, and to estimate diffuse reflectance parameters at each wavelength of a surface point, from spectral images, along with the separation.

Two methods have been described to estimate specular reflectance parameters, one with and the other without estimating Fresnel reflectance, from either unsaturated or saturated specular reflection components.

Experimental results with synthetic and measured reflection values, symmetric or asymmetric, have demonstrated that reflection values can be separated successfully, and that diffuse reflectance parameters for colors can be estimated accurately at each wavelength from spectral images using the separation method.

Experimental results with synthetic and separated specular reflection components at different saturation levels have revealed that specular reflectance parameters for gloss intensity and for surface roughness can be estimated satisfactorily using these methods.

8.2. Contributions

The ultimate aim in CG&CV is to realistically model surface characteristics, such as reflection properties, shape, and texture, of real objects, and there have been several contributions in the present dissertation to that aim.

First, spectral images of an object can be captured using a new measurement system with an imaging spectrograph, which is equipped with a monochrome CCD camera, and a light source that is rotated around the object. Using these spectral images, instead of RGB images, spectral reflectance of the object can be estimated as a function of wavelength. Based on accurate diffuse reflectance parameters estimated with this method, after removing the influence of illumination and the camera used for measurement, colors of the object can be reproduced realistically, without effects such as metamerism.

Second, reflection values can be separated successfully at low computation cost using the least squares method, based on the fact that intensity of specular reflection depends on illumination and viewing directions, whereas diffuse reflection is independent of viewing direction at each surface point. The new method requires neither color segmentation, nor any particular instrument such as a polarization filter, nor extra processes such as PCA analysis to select the two vectors of diffuse and specular reflection in a color space and creating EPI images, as in existing studies. Using the new method, diffuse reflectance parameters can be estimated accurately at each wavelength along with the separation.

Third, specular reflectance parameters for gloss intensity and for surface roughness can be estimated efficiently from either unsaturated or saturated specular reflection components. Up to now, most techniques to model and render reflection properties in CG&CV have been directed at removing specular reflection from images as a nuisance, since specular reflection plays an important role in evaluating realism in a synthetic object, which is rendered with input images measured in real illumination different from that in the virtual environment. Several techniques have been developed to estimate specular reflectance parameters, assuming input images to be unsaturated, either by controlling the intensity of illumination or by generating HDR images as input images with several images captured at different exposure times. However, there are difficulties in ensuring that input images are unsaturated. Using the new method, specular reflectance

parameters for surface roughness can be estimated accurately, and those for gloss intensity can be estimated by replacing values that are saturated due to the limited dynamic range of image detectors.

Fourth, without the need to generate HDR images using multiple raw images measured at different exposure times, or to incorporate special instruments such as a diffuser in the measurement system for attenuating intensity of illumination, raw images that are saturated can be also used to estimate diffuse reflectance parameters, specular reflectance parameters for gloss intensity and for surface roughness with sufficient accuracy.

Based on reflectance parameters estimated with these methods, reflection properties of an object can be reproduced, associated with illumination in a virtual environment such as a digital museum for cultural heritage, either with photometric or with functional realism, or with physical accuracy, according to needs.

In future studies, there are several subjects to be investigated:

1. Reproduce specular reflection interactively with movements of any one of the object, the light source or the viewer/camera, when the other two are fixed.

2. Recognize objects or materials based on spectral distribution of color and intensity of gloss.

The first example of future work is for exhibiting synthetic objects with realistic reflection properties in a virtual environment, such as in a digital museum or in an online shop, as they appear in the real world. This can be accomplished by tracking real-time movements of objects when they are manipulated by a person who tries to view the objects from different perspectives, or by tracking real-time motions of the person when he/she moves his/her body or part of it around to view objects, with immovable illumination in the virtual environment.

The second subject is another example in which to apply reflectance parameters of various objects or materials, which are accurately estimated with the methods described in the present dissertation. There are difficulties in recognizing color in RGB values because of metamerism; therefore, object/material recognition using spectral distribution of color can provide high speed and high

precision. Using intensity of gloss, the purity of materials can be determined in applications such as classifying ceramic objects.

Finally, these methods can be incorporated easily into existing modeling and rendering systems in CG&CV for realistic and functional graphics in virtual or augmented environments, based on accurate information about colors and gloss of real objects, with rapidly developing networking technology.

Acknowledgements

This work was completed under the supervision of Professor Kunihiro Chihara and Associate Professor Yoshitsugu Manabe of the Graduate School of Information Science at Nara Institute of Science and Technology (NAIST), with financial support from a Japanese Government (Monbukagakusho) Scholarship.

I first express my genuine thanks to Professors Chihara and Manabe, who have been giving me great support and encouragement throughout my Master's and Ph.D. study for five years. I have learned much from them about doing research and about Japanese culture.

I am grateful to Professor Naokazu Yokoya of the Graduate School of Information Science at NAIST for his valuable comments on my research as a member of my dissertation committee, and also at seminars throughout the five years.

I also thank Assistant Professors Yoshihiro Yasumuro and Masataka Imura, Secretaries Ms. Keiko Kawamoto and Ms. Masae Yamada, who have been supporting me during my time at NAIST. I have received great help from Dr. Yasushi Masuda, Dr. Hiroshi Sasaki, Dr. Kouichi Minami, and other colleagues, especially the members who have been learning with me in the Image Processing Laboratory at NAIST. Many special thanks to them all. I also give my sincere acknowledgments to the researchers William Rieken, Damien Douxchamps, Hamid Laga, Peter Antoniac and Jaakko Hyry for their considerate help and interesting discussions with me.

I give special thanks to Professor Ian Smith for his helpful comments and valuable time correcting my English in papers and presentations, and helping improve my English skills in general. I am also grateful to Professor Katsumasa Watanabe, who was in the Computing Architecture Laboratory, Assistant Professor Masayuki Kanbara in the Vision and Media Computing Laboratory, Associate Professor Kentaro Inui in the Computational Linguistics, and other people at NAIST, for their kind concern for me.

Many heartfelt thanks to my parents, brothers and sisters, and my Chinese and Japanese friends. Special thanks to Mr. Wakasugi Yoshinobu and his family, to Mr. Shin Tsugio and his family, both of whom have been giving me family-like support since I came to Japan, to Ataru Nakazawa, and to the people in the tea school of Chuguji, with whom I have spent a pleasant time for about three years.

Appendix

A. List of Abbreviations

ADC :	analog/digital converter
BRDF :	bidirectional reflectance distribution function
BTF :	bidirectional texture function
CCD :	charge coupled device
CG :	computer graphics
CG&CV :	computer graphics and computer vision
CMOS :	complementary metal-oxide semiconductor
CRT :	cathode-ray tube
CUReT :	Columbia-Utrecht Reflectance and Texture
CV :	computer vision
EPI :	epipolar plane image
HDR :	high dynamic range
LCDs :	liquid crystal displays
OLED :	organic light-emitter display
PCA :	principal component analysis
RGB :	red, green, and blue
SD :	standard deviation
SED :	surface-conduction electron-emitter display
SSD :	sum of the squares of the difference
VR&AR :	virtual reality and augmented reality

B. List of Symbols

λ :	wavelength
$E(\lambda)$:	spectral radiance of light
$L(\lambda)$:	spectral power distribution of illumination
$S(\lambda)$:	camera sensitivity
$O(\lambda)$:	spectral distribution of surface material
S :	S type receptor
M :	M type receptor
L :	L type receptor
$_k$:	kth type receptor
R_k :	response of kth type receptor
S_k :	sensitivity of kth type receptor
Λ :	range of visible wavelengths
$\omega_1, \omega_2, \omega_3$:	set of weighted values
R, G, B :	three primaries
$r(\lambda), g(\lambda), b(\lambda)$:	three color matching functions
$_p$:	surface point
I_p :	sensor response at p
O_p :	spectral reflectance of surface material at p
$n_1(\lambda), n_2(\lambda)$:	refractive indices of first and second medium
α_1 :	incident angle
α_2 :	refractive angle
P :	surface patch
ρ_{brdf} :	BRDF
θ, ϕ :	angular coordinate system
θ_i, ϕ_i :	incident angle and its azimuth angle
θ_r, ϕ_r :	reflected angle and its azimuth angle
$d\omega$:	solid angle
Ω :	hemisphere of directions
$E_p(\lambda)$:	outgoing radiance at P
$L_p(\lambda)$:	incoming radiance at P

$E_d(\lambda)$:	diffuse reflection components
$E_s(\lambda)$:	specular reflection components
$R_d(\lambda)$ or R_d :	diffuse reflectance parameter
R_s :	specular reflectance parameter for gloss intensity
σ :	specular reflectance parameter for surface roughness
$F(n(\lambda), \theta_i)$:	Fresnel reflectance
G :	geometrical attenuation factor
a :	absorption factor
$n(\lambda)$ or n :	refractive index of surface material
N :	unit vector of surface normal
H :	unit half-vector
L :	unit illumination vector
V :	unit viewing vector
α :	angle between N and H
$_j$:	incident position
$E(\lambda, \theta_r)$:	reflection value
$E'_d(\lambda)$:	measured reflection values
ε_d :	SSD between logarithm of $E'_d(\lambda)$ and of theoretical diffuse reflection component
$E_s(\lambda, \theta_r)$:	specular reflection components
$E'_{sj}(\lambda, \theta_r)$:	measured specular reflection components
ε_s :	SSD between logarithm of $E'_{sj}(\lambda, \theta_r)$ and of theoretical specular reflection component

C. List of Publications

Journal Papers

1. Shiying Li, Yoshitsugu Manabe and Kunihiro Chihara: A method for estimating specular reflectance parameters, *Transactions of the Institute of System, Control and Information Engineers*, vol.19, no.3, pp.31-33, 2006 (in Japanese).

International Conferences

1. Shiying Li, Yoshitsugu Manabe and Kunihiro Chihara: Estimating reflectance parameters of an object from saturated spectral images, *Proceedings of Computer Graphics, Imaging and Visualization*, pp.335-340, 2006.

2. Shiying Li, Yoshitsugu Manabe and Kunihiro Chihara: Estimating specular parameters from saturated spectral images, *Proceedings of IS&T/SPIE Conference on Electronic Imaging*, vol.6062, pp.606208.1-10, 2006.

3. Shiying Li, Yoshitsugu Manabe and Kunihiro Chihara: Color and gloss reproduction from multispectral images, *Proceedings IS&T/SPIE Conference on Electronic Imaging*, vol. 5667, pp.170-177, 2005.

Domestic Conferences in Japan

1. Shiying Li, Yoshitsugu Manabe and Kunihiro Chihara: Estimating reflectance parameters from saturated spectral images, *Proceedings of Meeting on Imaging Recognition and Understanding*, IS1-50, pp.606-611, 2006.

2. Shiying Li, Yoshitsugu Manabe, Kunihiro Chihara: Estimating reflectance parameters for color reproduction, *Proceedings of Conference on Color Science*, vol.30. pp.70-71, 2006.

3. Shiying Li, Yoshitsugu Manabe and Kunihiro Chihara: Modeling reflection properties using imaging spectrograph, *Proceedings of 49th Conference on System, Control and Information*, vol.49, pp.581-582, 2005.

4. Shiying Li, Yoshitsugu Manabe and Kunihiro Chihara: Estimating specular reflectance parameters, *Proceedings of Symposium on Visual Information, Information Processing Society in Kansai branch*, no.A-06, pp.23-24, 2004.

5. Shiying Li, Yoshitsugu Manabe and Kunihiro Chihara: Estimating Reflectance parameters using spectral images, *Proceedings of 48th Conference on System, Control and Information*, vol.48, 3050, pp.267-268, 2004.

6. Shiying Li, Yoshitsugu Manabe and Kunihiro Chihara: Measuring Reflection Properties at Objects Surface, *Proceedings of 46th Conference on Automatic Control*, FA2-08-5, pp.773-774, 2003.

7. Shiying Li, Yoshitsugu Manabe and Kunihiro Chihara: Measuring gloss and estimating reflectance parameters using spectral images, *Proceedings of 47th Conference on System, Control and Information*, vol.47, pp.315-316, 2003.

References

[1] Robert Siegel and John Howell: *Thermal Radiation Heat Transfer* (4th Edition), Taylor & Francis, 2002.

[2] David A. Forsyth and Jean Ponce: *Computer Vision: A Modern Approach*, Prentice Hall, 2003.

[3] Gerard Medioni and Singbing Kang: *Emerging Topics in Computer Vision*, Prentice Hall, 2005.

[4] Paul S. Hechbert: A survey of texture mapping, *IEEE Computer Graphics and Applications*, no.6, 1986.

[5] James P. Lewis: Algorithms for solid noise synthesis, *International Conference on Computer Graphics and Interactive Techniques (Proceedings of SIGGRAPH1989)*, vol.23, no.3, pp.263-270, 1989.

[6] Shiying Li: *Structural Analysis on the Developing Process of Texture Mapping in Scientific Papers and Patents*, Master's Thesis, ShinShu University, 2002 (in Japanese).

[7] Singbing Kang: A survey of image based rendering techniques, *Proceedings of Videometrics VI (SPIE International Symposium on Electronic Imaging: Science and Technology)*, vol.3641, pp.2-16, 1999.

[8] Stephen H. Westin, James R. Arvo and Kenneth E. Torrance: Predicting reflectance functions from complex surfaces, *International Conference on Computer Graphics and Interactive Techniques (Proceedings of SIGGRAPH1992)*, vol.26, no.2, pp.255-263, 1992.

[9] Pat Hanrahan and Wofgang Krueger: Reflection from layered surfaces due to subsurfaces scattering, *International Conference on Computer Graphics and Interactive Techniques (Proceedings of SIGGRAPH1993)*, pp.165-174, 1993.

[10] Jay S. Gondek, Gary W. Meyer and Jonathan G. Newman: Wavelength dependent reflectance functions, *International Conference on Computer Graphics and Interactive Techniques (Proceedings of SIGGRAPH1994)*, pp.213-220, 1994.

[11] Gregory J. Ward: Measuring and modeling anisotropic reflection, *International Conference on Computer Graphics and Interactive Techniques (Proceedings of SIGGRAPH1992)*, vol.26, no.2, pp.265-272, 1992.

[12] Kristin J. Dana, Bram Van Ginneken, Shree K. Nayar and Jan J. Koenderink: Reflectance and texture of real-world surfaces, *ACM Transactions on Graphics (Proceedings of SIGGRAPH1999)*, vol.18, no.1, pp.1-34, 1999.

[13] Yoichi Sato and Katsushi Ikeuchi: Temporal-color space analysis of reflection, *Journal of the Optical Society of America A*, vol.11, no.11, pp.2990-3002, 1994.

[14] Shree K. Nayar, Xi-Sheng Fang and Terrance Boult: Separation of reflection components using color and polarization, *International Journal of Computer Vision*, vol.21, no.3, pp.163-186, 1997.

[15] Yoichi Sato, Mark D. Wheeler and Katsushi Ikeuchi: Object shape and reflectance modeling from observation, *International Conference on Computer Graphics and Interactive Techniques (Proceedings of SIGGRAPH1997)*, vol.31, pp.379-388, 1997.

[16] Takashi Machida, Naokazu Yokoya, and Haruo Takemura: Surface reflectance modeling of real object with interreflections, *Proceedings of International Conference on Computer Vision*, vol.1, pp. 170-177, 2003.

[17] Robby T. Tan, and Katsushi Ikeuchi: Separating reflection components of textured surfaces using a single image, *IEEE Transactions on Pattern Analysis and Machine Intelligence*, vol.27, no.2, pp.178-193, 2005.

[18] Roy Hall: *Illumination and color in computer generated imagery*, Springer-Verlag, New York, 1989.

[19] Roy Hall: Comparing spectral color computation methods, *IEEE Computer Graphics and Applications*, vol.19, no.4, pp.36-45, 1999.

[20] Garrett M. Johnson and Mark D. Fairchild: Full-spectral color calculations in realistic image synthesis, *IEEE Computer Graphics and Applications*, vol.19, no.4, pp.1-7, 1999.

[21] Andrew S. Glassner: How to derive a spectrum from an RGB triplet, *IEEE Computer Graphics and Applications*, vol.9, no.4, pp.95-99, 1989.

[22] Reiner Lenz, Peter Meer and Markku Hauta-Kasari: Spectral-based illumination estimation and color correction, *Color Research and Application*, vol.24, no.2, pp. 98-111, 1998.

[23] Yinlong Sun, F. David Fracchia, Thoms W. Calvert and Mark S. Drew: Deriving spectra from colors and rendering light interference, *IEEE Computer Graphics and Applications*, vol.19, no.4, pp.61-67, 1999.

[24] Brian Smits: An RGB to spectrum conversion for reflectances, *Journal of Graphics Tools*, vol.4, no.4, pp.11-22, 1999.

[25] Yinlong Sun, F. David Fracchia, Mark S. Drew and Thomas W. Calvert: A spectrally based framework for realistic image synthesis, *The Visual Computer*, vol.17, no.7, pp.429-444, 2001.

[26] Norihiro Tanaka, Shoji Tominaga and Toshiyuki Kawai: A multi-channel camera and its application to estimation of a reflection model, *Display and Imaging*, vol.8, pp.283-291, 2000 (in Japanese).

[27] Shoji Tominaga, Norihiro Tanaka and Tkayuki Komada: Imaging and rendering of oil paintings using a multi-band camera, *Proceedings of IEEE Southwest Symposium on Image Analysis and Interpretation*, pp.6-10, 2004.

[28] Yoshitsugu Manabe and Seiji Inokuchi: Recognition of material types using spectral images, *Proceedings of International Conference on Pattern Recognition*, pp.840-843, 1996.

[29] Shinichi Kurosaka: *Simultaneous measurement system of 3D shape and surface spectral distribution*, Master's Thesis, Graduate School of Information Science, Nara Institute of Science and Technology, 2000.

[30] Yoshitsugu Manabe, Shinichi Kurosaka and Kunihiro Chihara: Simultaneous measurement system of spectral distribution and shape, *IEICE Transitions on Communications*, vol.J84-DII, no.6, pp.1012-1019, 2001 (in Japanese).

[31] Kate Devlin, Alan Chalmers, Alexander Wilkie and Werner Purgathofer: Tone reproduction and physically based spectral rendering, *Eurographics 2002*, pp. 101-123, 2002.

[32] Paul E. Debevec and Jitendra Malik: Recovering high dynamic range radiance maps from photographs, *International Conference on Computer Graphics and Interactive Techniques (Proceedings of SIGGRAPH1997)*, pp.369-378, 1997.

[33] Shree K. Nayar and Tomoo Mitsunaga: High dynamic range imaging: spatially varying pixel exposures, *Proceedings of IEEE Conference on Computer Vision and Pattern Recognition*, 2000.

[34] Shree K. Nayar and Vlad Branzoi: Adaptive dynamic range imageing: Optical control of pixel exposures over space and time, *Proceedings of the Ninth IEEE international Conference on Computer Vision*, pp.1-8, 2003.

[35] Wojciech Matusik, Hanspeter Pfister, Matt Brand and Leonard McMillan: A data-driven reflectance model, *ACM Transactions on Graphics (Proceedings of SIGGRAPH2003)*, vol.22, no.3, pp.759-769, 2003.

[36] Michael D. Grossberg and Shree K. Nayar: High dynamic range from multiple images: which exposures to combine?, *Proceedings of IEEE International Workshop on Color and Photometric Methods in Computer Vision*, pp.1-8, 2003.

[37] Shiying Li, Yoshitsugu Manabe, and Kunihiro Chihara: Color and gloss reproduction from multispectral images, *Proceedings IS&T/SPIE Conference on Electronic Imaging*, vol. 5667, pp.170-177, 2005.

[38] Shiying Li, Yoshitsugu Manabe and Kunihiro Chihara: Estimating specular parameters from saturated spectral images, *Proceedings of IS&T/SPIE Conference on Electronic Imaging*, vol.6062, pp.606208.1-10, 2006.

[39] Shiying Li, Yoshitsugu Manabe and Kunihiro Chihara: A method for estimating specular reflectance parameters, *Transactions of the Institute of System, Control and Information Engineers*, vol.19, no.3, pp.31-33, 2006.

[40] Shiying Li, Yoshitsugu Manabe and Kunihiro Chihara: Estimating reflectance parameters of an object from saturated spectral images, *Proceedings of Computer Graphics, Imaging and Visualisation*, pp.335-340, 2006.

[41] Margaret Hagen: *Varieties of realism*, Cambridge University Press, 1986.

[42] James A. Ferwerda: Three varieties of realism in computer graphics, *in Human Vision and Electronic Imaging VIII* (Bernice E. Rogowitz and Thrasyvoulos N. Pappas, Ed.), the International Society for Optical Engineering, 2003.

[43] Reynald Dumont, Fabio Pellacini and James A. Ferwerda: Perceptually-driven decision theory for interactive realistic rendering, *ACM Transactions on Graphics (Proceedings of SIGGRAPH2003)*, vol.22, no.2, pp.152-181, 2003.

[44] Steven A. Shafer: Using color to separate reflection components, *Color Research and Applications*, vol.10, pp.210-218, 1985.

[45] Johann Heinrich Lambert: *Photometria, sive de mensura de Gradibus luminis*, Colorum et umbrae, Augsberg, Germany, Eberhar Klett, 1760.

[46] Kenneth E. Torrance, and Ephraim M. Sparrow: Theory of off-specular reflection from roughened surfaces, *Journal of the Optical Society of America A*, vol.57, pp.1105-1114, 1967.

[47] Robert L. Cook and Kenneth E. Torrance: A reflectance model for computer graphics, *Computer Graphics (Proceedings of SIGGRAPH1981)*, vol.15, no.3, pp.307-316, 1981.

[48] Lawrence B. Wolff: Polarization-based material classification from specular reflection, *IEEE Transations on Pattern Analysis and Machine Intelligence*, vol.12, no.11, pp.1059-1071, 1990.

[49] Tongbo Chen, Michael Goesele and Hans-Peter Seidel: Mesostructure from specularity, *Proceedings of IEEE Computer Society Conference on Computer Vision and Patttern Recognition (CVPR)*, vol.2, pp.1825-1832, 2006.

[50] Gunter Wyszechi and W.S. Stiles: *Color science: Concepts and methods, quantitative data and formulae*, 2nd Edition, John Wiley & Sons, 1982.

[51] Graham Saxby: *The science of imaging*, IoP Publishing Ltd, 2002.

[52] Reinhard Klette, Karsten Schluns and Andreas Koschan: *Compter vision: Three-dimensional data from images*, Spinger-Verlag, Singapore, 2001.

[53] Jack Tumblin and Jessica K. Hodgins: Two methods for display of high contrast images, *ACM transactions on Graphics (Proceedings of SIGGRAPH1999)*, vol.18, no.1, pp.56-94, 1999.

[54] Greg Ward: High dynamic range imaging, *Proceedings of the Ninth Color Imaging Conference*, pp.9-16, 2001.

[55] Michael Oren and Shree K. Nayar: Generalization of the Lambertian model and inplications for machine vision, *International Journal of Computer Vision*, vol.14, no.3, 1996.

[56] Lawrence B. Wolff, Shree K. Nayar and Michael Oren: Improved diffuse reflection models for computer vision, *International Journal of Computer Vision*, vol.30, no.1, pp.55-71, 1998.

[57] Peter Beckmann and Andre Spizzichino: *The scattering of electromagnetic waves from rough surface*, Pergamon Press, 1963.

[58] Bui Tuong Phong: Illumination for computer generated pictures, *Communications of ACM*, vol.18, no.6, pp.311-317, 1975.

[59] Shree K. Nayar, Katsushi Ikeuchi and Takeo Kanade: Surface reflection: Physical and geometrical perspectives, *IEEE Transactions on Pattern Analysis and Machine Intelligence*, vol.13, no.7, pp.611-635, 1991.

[60] Xiao D. He, Kenneth E. Torrance, Francois X. Sillion and Donald P. Greenberg: A comprehensive physical model for light reflection, *Computer Graphics (Proceedings of SIGGRAPH1991)*, vol.25, no.5, pp.175-186, 1991.

[61] Eric P. F. Lafortune, Sing-Choong Foo, Kenneth E. Torrance and Donald P. Greenberg: Non-linear approximation of reflectance functions, *International Conference on Computer Graphics and Interactive Techniques (Proceedings of SIGGRAPH1997)*, pp.117-126, 1997.

[62] Michael Ashikhmin and Peter Shirley: An anisotropic Phong BRDF model, *Journal of Graphics Tools*, vol.5, no.2, pp.25-32, 2000.

[63] Stephen R. Marschner, Stephen H. Westin, Adam Arbree and Jonathan T. Moon: Measuring and modeling the appearance of finished wood, *ACM Transactions on Graphics (Proceedings of SIGGRAPH2005)*, pp.727-734, 2005.

[64] Thomas Leung and Jitendra Malik: Representing and recognizing the visual appearance of materials using three-dimensional textons, *International Journal of Computer Vision*, vol.43, no.1, pp.29-44, 2001.

[65] Xin Tong, Jindan Zhang, Ligang Liu, Xi Wang, Baining Guo and Heung-Yeung Shum: Synthesis of bidirectional texture functions on arbitrary surfaces, *ACM Transations on Graphics (Proceedings of SIGGRAPH2002)*, vol.21, pp.665-672, 2002.

[66] Stephen R. Marschner, Stephen H. Westin, Eric P. F. Lafortune and Kenneth E. Torrance: Image-based bidirectional reflection distribution function measurement, *Applied Optics*, vol.39, no.16, pp.2592-2600, 2000.

[67] Kristin J. Dana and Jing Wang: Device for convenient measurement of spatially varying bidirectional reflectance, *Journal of Optical Society of America A*, vol.21,, no.1, pp.1-12, 2004.

[68] Lawrence B. Wolff and Terrance Boult: Constraining object features using polarization reflectance model, *IEEE Transations on Pattern Analysis and Machine Intelligence*, vol.13, no.7, pp.35-657, 1991.

[69] Sylvia C. Pont and Jan J. Koenderink: Bidirectional reflectance distribution function of specular surfaces with hemispherical pits, *Journal of Optical Society of America A*, vol.19, no.12, pp.2456-2466, 2002.

[70] Gudrun J. Klinker, Steven A. Shafer and Takeo Kanade: The measurement of highlight in color images, *International Journal of Computer Vision*, vol.2, pp.7-32, 1988.

[71] Gudrun J. Klinker, Steven A. Shafer and Takeo Kanade: A physical approach to color image understanding, *International Journal of Computer Vision*, vol.4, pp.7-38, 1990.

[72] Norihiro Tanaka and Shoji Tominaga: Analysis and estimation of a three-dimensional reflection model, *Computer Vision and Image Media*, vol.41, no.SIG10, pp.1-11, 2000 (in Japanese).

[73] Antonio Criminisi, Sing Bing Kang, Rahul Swaminathan, Richard Szeliski and P. Anandan: Extracting layers and analyzing their specular properties using epipolar-plane-image analysis, *Computer Vision and Image Understanding*, vol.97, pp.51-85, 2005.

[74] Thanda Oo, Hiroshi Kawasaki, Yutaka Ohsawa and Katsushi Ikeuchi: Separation of reflection and transparency using epipolar plane image analysis, *Proceedings of the 7th Asian Conference on Computer Vision*, vol.1, pp.908-917, 2006.

[75] Katsushi Ikeuchi and Kosuke Sato: Determining reflectance properties of an object using range and brightness images, *IEEE Transactions on Pattern Analysis and Machine Intelligence*, vol.13, no.11, 1991.

[76] Kazuko Omata, Hideo Saito and Shinji Ozawa: Recovery of shape and surface reflectance of a specular object from relative rotation of light source, *IEICE Transactions on Communications*, D-II, vol.J83, no.3, pp.927-937, 2000.

[77] Michael Oren and Shree K. Nayar: A theory of specular surface geometry, *International Journal of Computer Vision*, vol.24, no.2, pp.105-124, 1996.

[78] James A. Ferwerda, Fabio Pellacini and Donald P. Greenberg: A psychophysically-based model of surface gloss perception, *Proceedings of SPIE Human Vision and Electronic Imaging*, pp.291-301, 2001.

[79] Takashi Machida: *Dense estimation of surface reflectance properties based on inverse rendering*, Ph.D. Dissertation, Graduate School of Information Science, Nara Institute of Science and Technology, 2005.

[80] Jing Wang and Kristin J. Dana: Relief texture from specularities, *IEEE Transactions on Pattern Analysis and Machine Intelligence*, vol.28, no.3, pp.446-457, 2006.

[81] Michael Bass (Ed.), Optical Society of America: *Handbook of Optics*, McGraw-Hill Professional, 1994.

[82] Elli Angelopoulou and Sofya Poger: Specular highlights of plastic surfaces and the Fresnel coefficient, *Proceedings of SPIE Conference on Imaging Display and Detectors*, vol.5578, pp.465-475, 2004.